JOURNAL OF COMPUTATIONAL PHYSICS 115, 249–266 (1994)

Simulation of Three-Dimensional Turbulent Flow in Non-Cartesian Geometry

DALIA FISHELOV

Institute of Mathematics, The Hebrew University, Jerusalem, Israel 91904

Received December 29, 1992; revised May 3, 1994

A three-dimensional simulation of turbulent (high Reynolds numbers) flow over a sphere was performed. We have applied vortex schemes by decomposing the physical region into two. The first is a thin layer near the sphere, where we have used a spherical coordinate system. The second is the rest of the physical domain, where we have applied the grid-free vortex method with a deterministic approximation to the viscous term. The results indicate constant growth in time of the L_2 norm of the vorticity and concentration of the vorticity field in small portions of the region.

1. INTRODUCTION

In this work we are interested in three-dimensional turbulent flow—a subject that attracted many mathematicians and engineers for several decades. The physical richness of turbulence and its yet unfounded full theory have been the reasons. To better understand the physics of transition to turbulence and turbulence itself, efforts have been made in several directions, such as theoretical work, physical experiments, and numerical simulations. Landau and Lifshitz [33], as well as Lin [34] and Drazin and Reid [25], observed that small perturbations on a steady-state solution of the Navier–Stokes equations may be unstable for high Reynolds numbers. In [33] Landau and Lifshitz characterize a fully developed turbulent flow as a superposition of turbulent eddies of different sizes. As the Reynolds number increases, eddies of every size are present. A statistical theory of homogeneous turbulence based on the correlation function was developed in [7, 20]. In [43, 21] it was observed that in regions where the vorticity is large in magnitude, it tends to align with a family of eigenvectors of the deformation matrix. It was also shown in [9, 37] that an initially smooth solution of Euler equations becomes singular at a finite time T^* if and only if the vorticity accumulates rapidly so that $\int_0^t |\xi|_\infty(s)\,ds$ tends to infinity as $t \to T^*$, where $|\xi|_\infty(s)$ is the infinity norm at time s. Avellaneda and Majda [3, 4], as well as Yakhot and Orszag [49], have recognized the need for renormalization for turbulent flow and developed a theory for a model linearized problem (advection–diffusion) in the steady, as well as the time dependent, case. In the vortex context—theory has dealt among other things with Hausdorff dimensions of the support of vorticity, vortex stretching, and hairpin formation. It was conjectured in [39, 40] that the Hausdorff dimension of the vorticity support for the class of turbulent flow is approximately 2.5—this is compatible with numerical results (see [17]) for the stretching of an initially perturbed vortex tube. Stretching of vortex lines [17, 18] and hairpin formation [19] were observed as well; it was shown in [18] that if vortex stretching occurs, in order to prevent the kinetic energy from increasing in time, vortex lines should fold and thus form hairpins of vorticity.

Measurements from experiments are available for flow in several geometries. Head and Bandyapodhyay [26] have performed experiments for the flow over a flat plate, indicating the formation of small hairpins of vorticity near the boundary. For the flow over a circular cylinder physical results are available from the experiments of Coutanceau and Bouard [23, 14]. A limited number of experiments were performed for a flow over a sphere and for other geometries. The drag coefficient for various Reynolds numbers was measured for a flow over a sphere and for a bowling ball entering water at various speeds (see [48; 6, Chaps. 5, 6].

The need for numerical simulations emerges from the fact that physical experiments are limited by their nature to specific geometries, initial and far-field conditions. Numerical results provide additional insight of the phenomena and a qualitative picture of the flow, which in turn may become a basis for further development in turbulence theory. In [16, 27] simulations for a flow over a flat plate in three-dimensional space were designed, and they indicate growth of boundary layer thickness, amplification of boundary layer disturbances, and formation of small vorticity hairpins. For the flow over a cylinder [44, 15] recirculation zones, main and secondary vortices were observed in the numerical simulations and they indicate similar visualizations of the flow derived from physical measurements. Numerical simulations include also tracking internal flows, such as the flow initiated by a single vortex located at the center of a two-dimensional box [5].

In this work we performed numerical experiments for slightly viscous flow over bodies with more complex geometry, such as a sphere. The problem for a flow over a sphere is interesting

0021-9991/94 $6.00

by its own right, since a sphere is a common geometry in nature as well as in artificial products. Moreover, it is a model for other three-dimensional problems of flow in complicated geometry, as one can either transform the computational domain to the exterior of a sphere, or use techniques similar to the ones utilized here. The problem for the flow over a sphere at high Reynolds numbers has—to my knowledge—no published numerical results.

The numerical methods that we used are vortex schemes; these methods are efficient for high Reynolds number flow, since they concentrate most of the computational elements in the region where the most interesting phenomena occur. Thus, for the flow over solid bodies, small scale phenomena are captured by the presence of many computational elements near the body, while away from the body, where large scale phenomena dominate, fewer computational elements reside. Moreover, there is no severe condition on the time step for vortex schemes (see [16, 1, 29]), since the methods are based on Lagrangian tracking of the vorticity field. Our numerical approximation consists of two parts; the first is the region away from the sphere, where we have approximated the Navier–Stokes equations; the second is the region near the sphere, where we have approximated the boundary layer equations. For the first, we have applied a vortex scheme that goes along the lines of the scheme suggested in [16], where for the stretching term of the Navier–Stokes equations we applied a vortex blob version, suggested in [1]. The viscous term is discretized via a deterministic scheme suggested in [28].

For the second region, we have derived the boundary layer equations for the velocity and the vorticity fields. We then covered the sphere by tiles which are formed by a spherical coordinate system, created vorticity on the sphere to satisfy the no-slip boundary condition, and let these particles evolve with time via a spherical representation of the boundary layer equations; viscosity is approximated via random walks. The innovation in this paper is the derivation of the boundary layer equations, and the construction of a spherical coordinate system that fits the sphere excellently and enables us to partition the sphere in a convenient way.

We were able to obtain a qualitative and quantitative picture of at least the intermediate and large scales of the solution. The resolution of very small scales of a three-dimensional flow may require refinement of the numerical parameters and technique, and therefore more powerful computers. The numerical solution indicates constant growth of vorticity in discrete L_1 and L_2 norms and construction of intense vorticity on sets of smaller support.

The paper is organized as follows. In Section 2 we represent the problem as a set of differential equations including boundary and initial conditions. We also refer to physical phenomena as well as the mathematical approach related to the class of problems which contain the transition to turbulence and turbulence itself. Section 3 is devoted to the derivation of the boundary layer equations in the vicinity of the sphere. In Sections 4 and 5 we describe the numerical scheme in the boundary layer and the interior, respectively. Implementation of boundary conditions is further expanded in Section 6. In Section 7 we discuss convergence properties of the scheme and in Section 8 we represent the numerical results.

2. THE PHYSICAL PROBLEM

We are interested in solutions of the incompressible Navier–Stokes equations for low viscosity, or alternatively, for high Reynolds numbers. It is well known that the transition to turbulence and turbulence may appear for this class of flow. We focus on three-dimensional flow over complicated geometries and, as an example, we have taken a flow over a sphere—a problem which is interesting by itself, and—to my knowledge—has no published numerical results yet. Problems with other geometries can be similarly treated by body-fitted coordinates in their vicinity.

We shall use the vorticity formulation for Navier–Stokes equations in Cartesian coordinates; the latter are obtained by taking the curl of the corresponding velocity-pressure formulation,

$$\frac{\partial \xi}{\partial t} + (\mathbf{u}\cdot\nabla)\xi = (\xi\cdot\nabla)\mathbf{u} + R^{-1}\nabla^2\xi, \tag{2.1a}$$

$$\operatorname{div}\mathbf{u} = 0; \tag{2.1b}$$

ξ and $\mathbf{u}$ are the vorticity and the velocity vectors, respectively, and $\nabla^2\xi$ is the Laplacian operator in cartesian coordinates. The physical domain is the exterior of a sphere of radius a, with the following far-field boundary condition

$$\mathbf{u} \to \mathbf{U} = (U, 0, 0) \quad \text{as } |\mathbf{x}| \to \infty, \tag{2.2}$$

where $(U, 0, 0)$ is the cartesian representation of $\mathbf{U}$.

The conditions on the sphere consist of the following no-leak and no-slip conditions. Let $\mathbf{n}$ and $\mathbf{t}$ be unit normal and tangential vectors to the surface of the sphere. The no-leak boundary condition

$$\mathbf{u}\cdot\mathbf{n} = 0 \tag{2.3a}$$

assures that the flow does not enter the solid sphere. The no-slip boundary condition

$$\mathbf{u}\cdot\mathbf{t} = 0 \tag{2.3b}$$

means that the tangential components of the velocity vector for the fluid is identical to those for the body and they are both zero, since the body is in rest. Conditions (2.3a)–(2.3b) together form the following boundary conditions:

$$\mathbf{u} = \mathbf{0} \quad \text{for } |\mathbf{x}| = a. \tag{2.4}$$

Initially, $\mathbf{u} = \mathbf{U} = (U, 0, 0)$ at $t = 0$.

Turbulent flow, as described in [33], is characterized by the presence of extremely irregular variation in the velocity field with time at each point, and a similar variation of the velocity between different points in space at a given instant. The velocity continuously fluctuates about some mean value, and the amplitude of variation is in general not small, compared with the magnitude of the velocity itself. If one perturbs a steady-state solution by an initially small perturbation, then to first order the perturbation must satisfy a set of linear partial differential equations, whose solution may grow in time for a high enough Reynolds number. A similar analysis for various geometries and far-field conditions was carried out by Lin [34] and Drazin and Reid [25]. Landau and Lifshitz also characterize fully developed turbulence, where the flow may be regarded as a superposition of turbulent eddies of different sizes, an eddy size being the order of magnitude of distances over which the velocity varies appreciably. For non-viscous turbulent flow all sizes of eddies appear, and the energy associated with each scale of eddy passes to smaller scales without dissipation. For a viscous flow, the energy associated with small enough eddies—of order $l/R^{3/4}$ or less—is transformed into heat; here l and R are typical length and the Reynolds number respectively.

For homogeneous flow the energy $E(k)$ associated with the modes of magnitude k is the integral over all the appropriate Fourier modes of the correlation function [7, 20]. The Kolmogorov hypothesis asserts that [33, 17] as R tends to infinity the energy spectrum behaves as

$$E(k) = C * \varepsilon^{2/3} k^{-5/3} \quad \text{for } L_0^{-1} < |k| < L_d^{-1} \text{ (the inertial range)},$$

where ε is the rate of energy dissipation, L_d is of order $L_0/R^{3/4}$, C is a universal constant, and L_0 is the typical length-scale of the large eddies.

In the vorticity context, looking at the rate of energy dissipation, we find that for incompressible flow, $\varepsilon = (d/dt) \int_{R^3} |\mathbf{u}|^2 \, d\mathbf{x} = -R^{-1} \int_{R^3} |\xi|^2 \, d\mathbf{x}$. Since the rate of energy dissipation is observed experimentally [17, 18] to be large at high Reynolds numbers too, the enstrophy $\int_{R^3} |\xi|^2 \, d\mathbf{x}$ must become extremely large at high Reynolds numbers; this illustrates the important role that vorticity plays for this class of problems. Another interesting aspect of the solution is its smoothness; a relation between non-smoothness of 3D solutions of incompressible Euler equations and the growth of vorticity norms was made in [9]. It was proven that if $\mathbf{u}(\mathbf{x}, 0)$ is a smooth incompressible velocity field with finite energy, which belongs to the Sobolev space $W^{s,2}(R^3) = H^s(R^3)$ for $s \geq 3$, then the solution becomes singular at a finite time T^* if and only if $\int_0^t |\xi|_\infty \, ds$ tends to infinity as t tends to T^*.

Since the vorticity grows in magnitude as time evolves [17], vorticity folding must occur [18] to prevent the kinetic energy from growing in time; this process is responsible for the formation of small hairpins of vorticity. Computational evidence [2, 47] supports the alignment of intense vorticity with the largest eigenvalue of the deformation matrix at short times; at larger times, intense vorticity tends to align with the middle eigenvalue, which was found to be positive in these regions. The numerical results were supported by a survey of a simple model [38], for which the velocity field and the pressure have a particular form and the vorticity and the deformation matrix depend solely on time. It was proved [38] that there exists T_1 so that for $t > T_1$ the vorticity, whose magnitude was assumed to grow constantly in time, aligns with the middle eigenvalue of the deformation matrix.

3. THE BOUNDARY LAYER EQUATIONS

The most delicate question that arises when one applies a numerical scheme to regions with complex geometries is how to approach the boundaries. For the flow over a sphere it seems most natural to fit this surface with a spherical coordinate system. In the context of vortex schemes for flow over solid bodies, an important question is how one should apply the no-leak and the no-slip boundary conditions. One of the common approaches [16, 15, 27] is to model the flow by the Navier–Stokes equations away from the body, and by the Prandtl equations near the surface of the body; the resulting scheme was found to be numerically appropriate to describe the flow. To obtain a boundary layer approximation in the vicinity of the sphere we shall first represent the Navier–Stokes (equations of motion), the velocity–vorticity relations, and the incompressibility equation in spherical coordinates. By assuming that there exists a boundary layer for which changes in the solution are most profound in the direction normal to the surface, we then derive the boundary layer equations.

Let us first express the Navier–Stokes equations in spherical coordinates. The velocity–pressure formulation for the Navier–Stokes equations in cartesian coordinates is

$$\frac{\partial \mathbf{u}}{\partial t} + (\mathbf{u} \cdot \nabla)\mathbf{u} = -\nabla p + R^{-1} \nabla^2 \mathbf{u},$$

where $\mathbf{u}$ is the cartesian reresentation of the velocity vector and p is the pressure. Love [36] was the first to express the strain tensor in a general curvilinear coordinate system. He expressed each cartesian derivative in terms of curvilinear ones and applied the result to the curvilinear representation of the velocity vector. This involves the derivation of derivatives of curvilinear unit vectors with respect to curvilinear derivatives. The resulting equations take the following form (which can be found also in Pai [42] and O'Neill and Chorlton [41]). Let $\mathbf{u} = (u_r, u_\theta, u_\phi)$ be the velocity vector in spherical coordinates and let d/dt be the material derivative;

thus, the Navier–Stokes equations can be written in spherical coordinates as

$$\frac{du_r}{dt} = -\frac{\partial p}{\partial r} + R^{-1}\left[\nabla^2 u_r - \frac{2}{r^2}\left(u_r + \frac{\partial u_\theta}{\partial \theta} + (\cot\theta)u_\theta + \frac{1}{\sin\theta}\frac{\partial u_\phi}{\partial \phi}\right)\right] \tag{3.1a}$$

$$\frac{du_\theta}{dt} = -\frac{1}{r}\frac{\partial p}{\partial \theta} + R^{-1}\left[\nabla^2 u_\theta + \frac{1}{r^2}\left(2\frac{\partial u_r}{\partial \theta} - \frac{u_\theta}{\sin^2\theta} - \frac{2\cos\theta}{\sin^2\theta}\frac{\partial u_\phi}{\partial \phi}\right)\right] \tag{3.1b}$$

$$\frac{du_\phi}{dt} = -\frac{1}{r\sin\theta}\frac{\partial p}{\partial \phi} + R^{-1}\left[\nabla^2 u_\phi + \frac{1}{r^2}\left(\frac{2}{\sin\theta}\frac{\partial u_r}{\partial \phi} + \frac{2\cos\theta}{\sin^2\theta}\frac{\partial u_\theta}{\partial \phi} - \frac{u_\phi}{\sin^2\theta}\right)\right]. \tag{3.1c}$$

The total derivatives may be written

$$\frac{du_r}{dt} = \frac{Du_r}{Dt} - \frac{u_\theta^2 + u_\phi^2}{r},$$

$$\frac{du_\theta}{dt} = \frac{Du_\theta}{Dt} + \frac{u_r u_\theta - (\cot\theta)u_\phi^2}{r},$$

$$\frac{du_\phi}{dt} = \frac{Du_\phi}{Dt} + \frac{u_r u_\phi + (\cot\theta)u_\theta u_\phi}{r},$$

where

$$\frac{D}{Dt} = \frac{\partial}{\partial t} + u_r\frac{\partial}{\partial r} + \frac{u_\theta}{r}\frac{\partial}{\partial \theta} + \frac{u_\phi}{r\sin\theta}\frac{\partial}{\partial \phi}.$$

The incompressibility condition takes the form in spherical coordinates,

$$\operatorname{div}\mathbf{u} = \frac{1}{r^2}\frac{\partial}{\partial r}(r^2 u_r) + \frac{1}{r\sin\theta}\frac{\partial}{\partial \theta}(u_\theta\sin\theta) + \frac{1}{r\sin\theta}\frac{\partial u_\phi}{\partial \phi} = 0. \tag{3.1d}$$

We assume that there exists a boundary layer of thickness δ, in which the solution changes more rapidly in the radial direction, compared to changes in the tangential directions. We assume that u_θ and u_ϕ are of order one; therefore, from the incompressibility condition, u_r is of order δ in the boundary layer, noting that $r = O(1)$. For the viscous terms to be comparable in order of magnitude to other terms, such as the time derivate of tangential components of the velocity, we have to require that $\delta = O(1/\sqrt{R})$. Thus, neglecting terms of order δ or less, we have

$$\frac{du_\theta}{dt} = -\frac{1}{r}\frac{\partial p}{\partial \theta} + R^{-1}\frac{\partial^2 u_\theta}{\partial r^2}, \tag{3.2a}$$

$$\frac{du_\phi}{dt} = -\frac{1}{r\sin\theta}\frac{\partial p}{\partial \phi} + R^{-1}\frac{\partial^2 u_\phi}{\partial r^2}, \tag{3.2b}$$

$$-\frac{u_\theta^2 - u_\phi^2}{r} = -\frac{\partial p}{\partial r}, \tag{3.2c}$$

$$\operatorname{div}\mathbf{u} = 0. \tag{3.2d}$$

Note that in the neighborhood of the poles $\theta = 0, \pi$ the spherical coordinate system is singular, thus Eqs. (3.1a)–(3.1d) are not valid in their usual sense, nor is the Prandtl approximation. Therefore, we shall use a local Cartesian coordinate system near the poles, and the surface of the sphere will be approximated by a small horizontal flat plate; the corresponding boundary layer approximation is well known and is described in detail in Section 4.

To proceed in deriving the boundary layer equations for the vorticity, we first write the vorticity vector in terms of the velocity field via a spherical representation:

$$\xi_r = \frac{1}{r^2\sin\theta}\left(\frac{\partial}{\partial \theta}(r u_\phi\sin\theta) - \frac{\partial}{\partial \phi}(r u_\theta)\right),$$

$$\xi_\theta = \frac{1}{r\sin\theta}\left(\frac{\partial}{\partial \phi}u_r - \frac{\partial}{\partial r}(r u_\phi\sin\theta)\right),$$

$$\xi_\phi = \frac{1}{r}\left(\frac{\partial}{\partial r}(r u_\theta) - \frac{\partial}{\partial \theta}u_r\right).$$

Neglecting lower order terms (of order less than $1/\delta$) in the boundary layer, we have

$$\xi_r = 0, \quad \xi_\theta = -\frac{\partial u_\phi}{\partial r}, \quad \xi_\phi = \frac{\partial u_\theta}{\partial r}. \tag{3.3}$$

Upon differentiation of the boundary layer equations (3.2a)–(3.2b) with respect to r, using (3.3) and (3.2c) and neglecting the stretching terms, we find

$$\frac{d\xi_\theta}{dt} = R^{-1}\frac{\partial^2 \xi_\phi}{\partial r^2}, \tag{3.4a}$$

$$\frac{d\xi_\phi}{dt} = R^{-1}\frac{\partial^2 \xi_\phi}{\partial r^2}, \tag{3.4b}$$

$$\operatorname{div}\mathbf{u} = 0. \tag{3.4c}$$

Note that the boundary-layer equations are not uniformly valid approximations to the Navier–Stokes equations, since the assumptions that the flow is nearly parallel to the body are false near separation and stagnation points. However, our numerical boundary is much thinner (of order $\sqrt{2\,\Delta t/R}$) than the physical

one suggested here (see Section 4) and is used merely to apply the boundary conditions more accurately.

4. THE NUMERICAL SCHEME IN THE BOUNDARY LAYER

The boundary layer equations were developed in the last section for the region $a < r < b$, where a is the radius of the sphere and $b - a \leq O(R^{-1/2})$. We actually use these equations in a much thinner layer, which is of order $\sqrt{2\,\Delta t/R}$, where Δt is the time step; we shall expand upon this choice later in this section. We describe here the numerical scheme for the approximation of the boundary layer equations (3.4a)–(3.4c), together with the no-leak and the no-slip boundary conditions (2.3a)–(2.3b).

We time-split the Prandtl equations (3.4a)–(3.4c) to non-viscous and viscous parts, where the non-viscous part is

$$\frac{d\xi}{dt} = 0, \quad \operatorname{div} \mathbf{u} = 0, \tag{4.1}$$

and the viscous one is

$$\frac{\partial \xi}{\partial t} = R^{-1} \frac{\partial^2 \xi}{\partial r^2}. \tag{4.2}$$

Here ξ denotes the non-zero components of the vorticity vector, i.e., $\xi = (\xi_\theta, \xi_\phi)$. For the non-viscous part (4.1) the particles are evolved according to their velocities, keeping the vorticity components as material quantities, i.e.,

$$\frac{d\mathbf{x}}{dt} = \mathbf{u}, \quad \operatorname{div} \mathbf{u} = 0,$$

$$\frac{d\xi}{dt} = 0.$$

For the viscous part, Eq. (4.2) is stepped in time via a random process that will be described later in this section.

Let us continue the description of the scheme for the inviscid step. First, we cover the surface of the sphere by tiles, which are formed by the spherical coordinate system. These tiles, which have varying areas in Cartesian coordinates, form a uniform mesh in the (θ, ϕ) plane. The evolution equations for particle locations must be written in spherical coordinates; thus

$$\frac{dr}{dt} = u_r, \quad \frac{d\theta}{dt} = \frac{1}{r} u_\theta, \quad \frac{d\phi}{dt} = \frac{1}{r \sin \theta} u_\phi, \quad \operatorname{div} \mathbf{u} = 0 \tag{4.3}$$

$$\frac{d\xi}{dt} = 0. \tag{4.4}$$

The velocity vector (u_r, u_θ, u_ϕ) may be derived from the vorticity vector by (3.3) as

$$u_\theta(r, \theta, \phi, t) = u_{\theta,\infty}(\theta, \phi, t) - \int_r^\infty \xi_\phi(r', \theta, \phi, t)\, dr', \tag{4.5}$$

$$u_\phi(r, \theta, \phi, t) = u_{\phi,\infty}(\theta, \phi, t) + \int_r^\infty \xi_\theta(r', \theta, \phi, t)\, dr'. \tag{4.6}$$

Here $u_{\theta,\infty}$ and $u_{\phi,\infty}$ are the θ and ϕ components of the velocity vector at $r = b$, which corresponds to the radius at which the thin boundary layer and the rest of the physical domain are matched. Similarly, by integration from r to ∞ we mean integration from r to b.

The radial component of the velocity, u_r, is derived from u_θ and u_ϕ by the incompressibility condition (3.1d). Upon requiring that $u_r = 0$ on the sphere (r = a), we obtain

$$r^2 u_r = -\int_a^r \frac{r'}{\sin\theta} \frac{\partial}{\partial \theta} (u_\theta \sin\theta)\, dr' - \int_a^r \frac{r'}{\sin\theta} \frac{\partial u_\phi}{\partial \phi}\, dr', \tag{4.7}$$

where a is the radius of the sphere.

The integrals in (4.5)–(4.6) can be approximated by $\frac{1}{2}(\xi_\phi)_i\, \Delta r + \sum_j (\xi_\phi)_j d_j f_j\, \Delta r$ and $\frac{1}{2}(\xi_\theta)_i\, \Delta r + \sum_j (\xi_\theta)_j d_j f_j\, \Delta r$, respectively, where

$$d_j = 1 - \frac{|\theta_i - \theta_j|}{\Delta\theta}, \quad f_j = 1 - \frac{|\phi_i - \phi_j|}{\Delta\phi}$$

are smoothing functions, and the summations are over all tiles T_j for which $0 \leq d_j \leq 1$, $0 \leq f_j \leq 1$, and $r_j \geq r_i$. Now let Δr tend to zero in such a way that $(\xi_\phi)_j\, \Delta r$ and $(\xi_\theta)_j\, \Delta r$ tend to finite values $(\tilde{\tau}_\phi)_j$ and $(\tilde{\tau}_\theta)_j$, respectively. Thus, (4.5)–(4.6) can be approximated by

$$(\tilde{u}_\theta)_i = \tilde{u}_\theta(r_i, \theta_i, \phi_i, t) = u_{\theta,\infty}(\theta_i, \phi_i, t) - \tfrac{1}{2}(\tilde{\tau}_\phi)_i - \sum_j (\tilde{\tau}_\phi)_j d_j f_j, \tag{4.8}$$

$$(\tilde{u}_\phi)_i = \tilde{u}_\phi(r_i, \theta_i, \phi_i, t) = u_{\phi,\infty}(\theta_i, \phi_i, t) + \tfrac{1}{2}(\tilde{\tau}_\theta)_i + \sum_j (\tilde{\tau}_\theta)_j d_j f_j, \tag{4.9}$$

where the summations in (4.8)–(4.9) are over all tiles T_j for which $0 \leq d_j \leq 1$, $0 \leq f_j \leq 1$, and $r_j \geq r_i$.

Similarly, from (4.7).

$$(\tilde{u}_r)_i = \tilde{u}_r(r_i, \theta_i, \phi_i, t) = -\frac{1}{r_i^2}\left[\frac{r_i^2 - a^2}{2} u_{\theta,\infty} \cot\theta_i\right] - \frac{\cot\theta_i}{r_i^2} L - \frac{1}{r_i^2}\left[\frac{I_+ - I_-}{\Delta\theta} - \frac{J_+ - J_-}{\Delta\phi}\right],$$

where

$$I_{\pm} = \frac{r_i^2 - a^2}{2} u_{\theta,\infty}(\theta_i \pm \Delta\theta/2, \phi_i, t) - \sum_{\pm}^{\theta} \frac{(r_j^*)^2 - a^2}{2} (\tilde{\tau}_\phi)_j d_j^{\pm} f_j,$$

$$J_{\pm} = \frac{r_i^2 - a^2}{2 \sin\theta_i} u_{\phi,\infty}(\theta_i, \phi_i \pm \Delta\phi/2, t) + \sum_{\pm}^{\phi} \frac{(r_j^*)^2 - a^2}{2} (\tilde{\tau}_\theta)_j d_j f_j^{\pm},$$

$$L = \sum_j \frac{(r_j^*)^2 - a^2}{2} (\tilde{\tau}_\phi)_j d_j f_j,$$

and

$$d_j^{\pm} = 1 - \frac{|\theta_j \pm \Delta\theta/2 - \theta_i|}{\Delta\theta}, \quad f_j^{\pm} = 1 - \frac{|\phi_j \pm \Delta\phi/2 - \phi_i|}{\Delta\phi},$$

$$r_j^* = \min(r_i, r_j).$$

The sums $\sum_+^\theta, \sum_-^\theta$ are over all T_j, such that $0 \le f_j \le 1$, and $0 \le d_j^+ \le 1$, $0 \le d_j^- \le 1$, respectively. Similarly the sums $\sum_+^\phi, \sum_-^\phi$ are over all T_j, such that $0 \le d_j \le 1$, and $0 < f_j^+ \le 1$, $0 \le f_j^- \le 1$, respectively. This is a thin radial layer, and therefore the number of operations to calculate the velocity fields for the tile method is $O(N)$, where N is the total number of tiles.

In order to include viscous effects in the neighborhood of the sphere, each particle undergoes a Gaussian random walk—a process that mimics the heat equation. The heat equation for the vorticity vector in the Prandtl formulation is

$$\frac{\partial \xi}{\partial t} = R^{-1} \frac{\partial^2 \xi}{\partial r^2}, \quad \xi = (\xi_\theta, \xi_\xi).$$

We step the solution in time by moving the centers of the tiles with Gaussian random walks (see [16]) in the radial direction only,

$$\bar{r}_i^{n+1} = \bar{r}_i^n + \eta(\Delta t, R);$$

here $\eta(\Delta t, R)$ is Gaussian random variable with mean zero and variance $2\,\Delta t/R$.

The no-slip boundary condition is then approximated by creating vorticity on the surface of the sphere (see [16]). Thus one looks at (4.8)–(4.9) applied on $r = a$ at certain collocation points and add an extra term to each of the sums therein; the extra term is associated with the vorticity which is created on the surface of the sphere. We require that with the additional terms—the right-hand sides of (4.8) and (4.9)—vanish at the selected collocation points. In other words, ξ_ϕ and ξ_θ (or, alternatively, $\tilde{\tau}_\phi$ and $\tilde{\tau}_\theta$) are created such that

$$\tilde{\tau}_\phi(a, \theta_i, \phi_j, t) = u_{\theta,\infty}(\theta_i, \phi_i, t) - \sum_j (\tilde{\tau}_\phi)_j d_j f_j, \tag{4.10a}$$

$$\tilde{\tau}_\theta(a, \theta_i, \phi_i, t) = -u_{\phi,\infty}(\theta_i, \phi_i, t) - \sum_j (\tilde{\tau}_\phi)_j d_j f_j, \tag{4.10b}$$

where the sums are taken over all j such that $0 \le d_j \le 1$, $0 \le f_j \le 1$, and $r_j \ge a$. For the convergence of the random process, we require that the maximum strength of vorticity created on the sphere will not exceed a prescribed amount, $\tilde{\tau}_{\max}$. As $\tilde{\tau}_{\max}$ tends to zero, The number of tiles tends to infinity and the error associated with the viscous term will decrease to zero (see Section 7) with high probability, provided that Δt and $\Delta\theta$, $\Delta\phi$ tend to zero (this results from numerical evidents for calculations over a flat plate and from the analysis of a simpler mode).

In a small neighborhood of poles $\theta = 0, \pi$ one needs to handle the singularity of the spherical coordinate system, and it is therefore advisable to use a local Cartesian coordinate system. We represent the vorticity and velocity vectors in Cartesian coordinates $\xi = (\xi_1, \xi_2, \xi_3)$ and $\mathbf{u} = (u, v, w)$, respectively. Writing the relation $\xi = \nabla \times \mathbf{u}$ in cartesian coordinates yields

$$\xi_1 = \frac{\partial w}{\partial y} - \frac{\partial v}{\partial z}, \quad \xi_2 = \frac{\partial u}{\partial z} - \frac{\partial w}{\partial x}, \quad \xi_3 = \frac{\partial v}{\partial x} - \frac{\partial u}{\partial y}.$$

Neglecting lower order terms (tangential derivatives) in the boundary layer yields

$$\xi_1 = -\frac{\partial v}{\partial z}, \quad \xi_2 = \frac{\partial u}{\partial z}, \quad \xi_3 = 0.$$

Integration with respect to z in the boundary layer gives

$$v(x, y, z, t) = v_\infty(x, y, t) + \int_z^\infty \xi_1(x, y, z', t)\, dz',$$

$$u(x, y, z, t) = u_\infty(x, y, t) - \int_z^\infty \xi_2(x, y, z', t)\, dz'.$$

Here $z = \infty$ refers to the vertical point where the interior domain matches the boundary layer and the horizontal velocities, respectively, u_∞, v_∞ refers to values of u and v for this z. The vertical component w of the velocity vector is recovered from the incompressibility condition,

$$w(x, y, z, t) = -\int_a^z \left(\frac{\partial u}{\partial x} + \frac{\partial v}{\partial y}\right)(x, y, z', t)\, dz'.$$

In the expressions above ξ_1, ξ_2 are derived from the spherical representation of ξ by the relations

$$\xi_1 = \xi_r \sin\theta\cos\phi + \xi_\theta \cos\theta\cos\phi - \xi_\phi \sin\phi, \tag{4.11a}$$

$$\xi_2 = \xi_r \sin\theta\sin\phi + \xi_\theta \cos\theta\sin\phi + \xi_\phi \cos\phi, \tag{4.11b}$$

$$\xi_3 = \xi_r \cos\theta + \xi_\theta \sin\theta, \tag{4.11c}$$

where we have neglected ξ_r in the boundary layer. The numerical approximations of the formulas above are similar but simpler than the ones in spherical coordinates and can be found in [27]. For the sake of completeness we quote them here. Let $\tilde{\tau}_1$ and $\tilde{\tau}_2$ approximate $\xi_1 \Delta z$ and $\xi_2 \Delta z$, respectively, as Δr tends to zero; thus

$$u_i = \tilde{u}(x_i, y_i, z_i, t) = u_\infty(x_i, y_i, t) - \tfrac{1}{2}(\tilde{\tau}_2)_i - \sum_j (\tilde{\tau}_2)_j d_j f_j,$$

$$v_i = \tilde{v}(x_i, y_i, z_i, t) = v_\infty(x_i, y_i, t) + \tfrac{1}{2}(\tilde{\tau}_1)_i + \sum_j (\tilde{\tau}_1)_j d_j f_j,$$

where $d_j = 1 - |x_i - x_j|/h_1$ and $f_j = 1 - |y_i - y_j|/h_2$ are smoothing functions, the summations are over all T_j for which $0 \le d_j \le 1$, $0 \le f_j \le 1$, and $z_j \ge z_i$. Similarly,

$$w_i = \tilde{w}(x_i, y_i, z_i, t) = -\frac{I_+ - I_-}{h_1} - \frac{J_+ - J_-}{h_2},$$

where

$$I_\pm = (z_i - a)u_\infty(x_i \pm h_1/2, y_i, t) - \sum\nolimits_\pm^x (\tilde{\tau}_2)_j d_j^\pm f_j z_j^*,$$

$$J_\pm = (z_i - a)v_\infty(x_i, y_i \pm h_2/2, t) + \sum\nolimits_\pm^x (\tilde{\tau}_1)_j d_j f_j^\pm z_j^*,$$

and

$$d_j^\pm = 1 - \frac{|x_i \pm h_1/2 - x_j|}{h_1}, \quad f_j^\pm = 1 - \frac{|y_i \pm h_2/2 - y_j|}{h_2},$$

$$z_j^* = \min(z_i, z_j).$$

The sums $\sum_+^x, \sum_-^x$ are over all T_j, such that $0 \le f_j \le 1$, and $0 \le d_j^+ \le 1$, $0 \le d_j^- \le 1$, respectively. Similarly the sums $\sum_+^y, \sum_-^y$ are over all T_j, such that $0 \le d_j \le 1$, and $0 \le f_j^+ \le 1$, $0 \le f_j^- \le 1$, respectively; we have chosen $h_1 = h_2 = h_\theta$.

When a spherical tile leaves a prescribed thin numerical boundary layer of order $\sqrt{2\,\Delta t/R}$, it becomes a blob, whose trajectory is described in the next section. Since we want to assure that with high probability a tile created on the boundary leaves the prescribed numerical boundary layer within several (one or two) time steps, we have chosen the numerical boundary layer to be of order $\sqrt{2\,\Delta t/R}$. The Cartesian components of the newly created vorticity blobs can be found by (4.11a)–(4.11c). And vice versa, a blob which enters the numerical boundary layer becomes a tile, where its tangential vorticity components can be recovered from its Cartesian ones and its radial component is set to zero.

5. THE NUMERICAL SCHEME IN THE INTERIOR

The boundary layer equations are used in a neighborhood $a \le r \le b$ of the sphere, where $b - a \le O(\sqrt{2\,\Delta t/R})$. Away from the sphere, for $r \ge b$, the Navier–Stokes equations are approximated by a three-dimensional vortex scheme [1, 16, 27]. It is possible to derive a vortex scheme for (2.1)–(2.3) with various choices of coordinate system; however, the Cartesian one is the simplest and the most adequate, since the velocity–vorticity relations as well as the differential equations and far-field conditions can be most easily represented in Cartesian coordinates.

We invoke the vorticity formulation of the Navier–Stokes equations, which is represented as follows. Along particle trajectories

$$\frac{d\mathbf{x}}{dt} = \mathbf{u}, \tag{5.1}$$

the vorticity is evolved via

$$\frac{d\xi}{dt} = (\xi \cdot \nabla)\mathbf{u} + R^{-1}\nabla^2 \xi. \tag{5.2}$$

Here $d/dt = \partial/\partial t + \mathbf{u} \cdot \nabla$ denotes the material derivative.

Let us represent $\mathbf{u}$ in terms of ξ. Since the flow is incompressible, there exists a vector valued function ψ, called the vector potential, such that $\mathbf{u} = \nabla \times \psi$. Note that ψ is determined up to an additive potential field ∇g, thus ψ can be chosen such that div $\psi = 0$. Upon taking the curl of the relation $\mathbf{u} = \nabla \times \psi$, we find that, since ψ is divergence-free,

$$\nabla^2 \psi = -\xi.$$

The last differential equation, together with a vanishing condition for the first-order derivatives of ψ at infinity, can be solved in R^3 by means of the Green's function $-G(\mathbf{x}) = 1/4\pi|\mathbf{x}|$ for the Laplacian operator, i.e.,

$$\psi(\mathbf{x}, t) = \int G(\mathbf{x} - \mathbf{x}')\xi(\mathbf{x}', t)\, d\mathbf{x}', \quad G(\mathbf{x}) = -1/4\pi|\mathbf{x}|.$$

The velocity $\mathbf{u}$ can be recovered by taking the curl of ψ,

$$\mathbf{u}(\mathbf{x}, t) = \int K(\mathbf{x} - \mathbf{x}')\xi(\mathbf{x}', t)d\mathbf{x}', \tag{5.3}$$

where $K(\mathbf{x})$ is the 3×3 matrix,

$$K(\mathbf{x}) = -\frac{1}{4\pi r^3}\begin{pmatrix} 0 & -z & y \\ z & 0 & -x \\ -y & x & 0 \end{pmatrix},$$

and $r = |\mathbf{x}| = \sqrt{x^2 + y^2 + z^2}$. Here we have accounted only for the condition of vanishing velocity at infinity. Note that (5.3) holds and implies indeed a vanishing velocity at infinity

as long as the vorticity has compact support, or alternatively, if it decayes as r^{-3} as r tends to infinity.

If we want to satisfy a non-homogeneous far-field condition for $\mathbf{u}$, we must add a potential flow ∇g, i.e., $\mathbf{u} = \nabla g + K * \xi$, where ∇g tends to $\mathbf{U}$ at infinity, leaving the no-leak boundary condition unchanged. Thus, we write

$$\mathbf{u} = \mathbf{u}_{\text{potential}} + K * \xi, \tag{5.4}$$

where $\mathbf{u}_{\text{potential}} = \nabla g$ and g is the potential function that satisfies $\nabla^2 g = 0$ in the domain $a < r < \infty$, ∇g tends to $\mathbf{U}$ as r tends to infinity, and $\partial g/\partial r = 0$ on the surface of the sphere ($r = a$). Here $\mathbf{U} = (U, 0, 0)$ represents uniform velocity in the x direction. Solving the Laplace equation with the appropriate boundary conditions for g yields

$$g = Ur \sin\theta \cos\phi(1 + a^3/2r^3).$$

In fact, one can pick g such that the no-leak boundary condition (2.3a) is satisfied on the body by requiring that $\partial g/\partial n = -(K * \xi) \cdot \mathbf{n}$ on the body. However, since we are approaching the sphere with the boundary layer equations, and the no-leak boundary condition is already imposed there, we only require that g leaves $\mathbf{u} \cdot \mathbf{n}$ unchanged.

5.1. *Spatial Discretization*

The singular kernel K is smoothed [16] via its convolution with a cutoff function ϕ_δ, where δ is the cutoff parameter. Denote by K_δ the smoothed kernel $K * \phi_\delta$; the latter is then explicitly differentiated [1] to approximate the stretching term $(\xi \cdot \nabla)(K * \xi)$ in (5.2) by $(\xi \cdot \nabla)(K_\delta * \xi)$. The viscous term $R^{-1}\nabla^2\xi$ is discretized in a similar manner; the vorticity is first convoluted with a cutoff function, and the approximation to the viscous term is then obtained by the convolution of the explicit Laplacian of the cutoff function with the vorticity, i.e., by $\nabla^2\phi_\delta * \xi$. This describes a deterministic approximation to the viscous term that we have suggested in [28]. All convolutions are then replaced by trapezoidal sums, which retain their initial accuracy on a uniform grid by the incompressibility condition. Since at each time level the Lagrangian mesh forms a flow map of an originally uniform spherical mesh, the formal accuracy of the trapezoidal rule is kept throughout the time-evolution of the mesh. Thus, the evolution of approximate particle locations $\tilde{\mathbf{x}}_i(t)$ is determined by the following system of ordinary differential equations:

$$\frac{d\tilde{\mathbf{x}}_i(t)}{dt} = \mathbf{u}_{\text{potential}}(\tilde{\mathbf{x}}_i(t)) + \sum_j K_\delta(\tilde{\mathbf{x}}_i(t) - \tilde{\mathbf{x}}_j(t))\tilde{\tau}_j(t)a_j, \tag{5.5}$$

$$\frac{d\tilde{\tau}_i(t)}{dt} = (\tilde{\tau}_i(t) \cdot \nabla)\left[\mathbf{u}_{\text{potential}}(\tilde{\mathbf{x}}_i(t)) + \sum_j K_\delta(\tilde{\mathbf{x}}_i(t) - \tilde{\mathbf{x}}_j(t))\tilde{\tau}_j(t)a_j\right] + R^{-1}\sum_j \nabla^2\phi_\delta(\tilde{\mathbf{x}}_i(t) - \tilde{\mathbf{x}}_j(t))\tilde{\tau}_j(t)a_j. \tag{5.6}$$

Here ∇ and ∇^2 represent Eulerian explicit differentiation, and

$$a_j = a^2\,\Delta\theta\,\Delta\phi(\sin\theta_j)_{\text{original}},$$

where its multiplication by Δr represents the volume of the original element created on the boundary; the latter is preserved by the incompressibility condition. Note also that

$$\mathbf{u}_{\text{potential}} = \nabla\left(Ur\sin\theta\cos\phi\left(1 + \frac{a^3}{2r^3}\right)\right) = \nabla\left(Ux\left(1 + \frac{a^3}{2r^3}\right)\right),$$

or in Cartesian components (u, v, w)

$$u_{\text{potential}} = U\left(1 + \frac{a^3(r^2 - 3x^2)}{2r^5}\right),$$

$$v_{\text{potential}} = -U\frac{3xya^3}{2r^5},$$

$$w_{\text{potential}} = -U\frac{3xza^3}{2r^5}.$$

To satisfy the no-leak boundary condition, for each blob located at $\tilde{\mathbf{x}}$ in the physical domain with centered vorticity $\tilde{\xi}$ one adds an imaginary blob at $\tilde{\mathbf{y}}$ inside the ball, with vorticity $\tilde{\xi}' = -\tilde{\xi}/|\tilde{\mathbf{x}}|$. The imaginary point lies on the straight line connecting $\tilde{\mathbf{x}}$ with the origin, such that $|\tilde{\mathbf{x}}|\,|\tilde{\mathbf{y}}| = a^2$. If we look now at the equation which relates the vorticity with the vector stream function ψ, $\nabla^2\psi = -\xi$, the solution $\psi = G * \xi$, where $G(\mathbf{x}) = -1/4\pi|\mathbf{x}|$, satisfies $\psi = 0$ on $r = a$ after the addition of the set of imaginary vortices. This, in turn, yields that $(\nabla \times \psi) \cdot \mathbf{n} = 0$, which means that $\mathbf{u} \cdot \mathbf{n} = 0$ on $r = a$.

Equations (5.5)–(5.6) take the following form after the addition of imaginary blobs:

$$\begin{aligned}
\frac{d\tilde{\mathbf{x}}_i(t)}{dt} &= \mathbf{u}_{\text{potential}}(\tilde{\mathbf{x}}_i(t)) + \sum_j K_\delta(\tilde{\mathbf{x}}_i(t) - \tilde{\mathbf{x}}_j(t))\tilde{\tau}_j(t)a_j \\
&\quad - \sum_j K_\delta(\tilde{\mathbf{x}}_i(t) - \tilde{\mathbf{y}}_j(t))\frac{\tilde{\tau}_j(t)}{|\tilde{\mathbf{x}}_j(t)|}a_j, \\
\frac{d\tilde{\tau}_i(t)}{dt} &= (\tilde{\tau}_i(t) \cdot \nabla)\mathbf{u}_{\text{potential}}(\tilde{\mathbf{x}}_i(t)) \\
&\quad + \tilde{\tau}_i \cdot \left[\sum_j \nabla K_\delta(\tilde{\mathbf{x}}_i(t) - \tilde{\mathbf{x}}_j(t))\tilde{\tau}_j(t)a_j\right. \\
&\quad \left. - \sum_j \nabla K_\delta(\tilde{\mathbf{x}}_i(t) - \tilde{\mathbf{y}}_j(t))\frac{\tilde{\tau}_j(t)}{|\tilde{\mathbf{x}}_j(t)|}a_j\right] \\
&\quad + R^{-1}\sum_j \nabla^2\phi_\delta(\tilde{\mathbf{x}}_i(t) - \tilde{\mathbf{x}}_j(t))\tilde{\tau}_j(t)a_j \\
&\quad - R^{-1}\sum_j \nabla^2\phi_\delta(\tilde{\mathbf{x}}_i(t) - \tilde{\mathbf{y}}_j(t))\frac{\tilde{\tau}_j(t)}{|\tilde{\mathbf{x}}_j(t)|}a_j.
\end{aligned} \tag{5.7}$$

Here

$$\tilde{\tau}\cdot\nabla K_\delta = \tilde{\tau}^x\frac{\partial}{\partial x}K_\delta + \tilde{\tau}^y\frac{\partial}{\partial y}K_\delta + \tilde{\tau}^z\frac{\partial}{\partial z}K_\delta,$$

where $\tau = (\tau^x, \tau^y, \tau^z)$ is the Cartesian representation of τ. It is desirable to cover the computational domain with blobs, for which some may carry zero vorticity initially. However, this will make our calculations unaffordable, and vorticity spreading is taken care of by the generation of new computational points on the wall, their convection and redistribution by (5.7).

5.2. *Temporal Discretization*

Time-derivatives appearing in (5.7) are approximated via a second-order Strang-type scheme (see, e.g., [27]). By (5.4) $\mathbf{u} = \mathbf{u}(\mathbf{x}, \xi)$, thus Eqs. (5.1)–(5.2) can be written in the form

$$\frac{d\mathbf{x}}{dt} = A(\mathbf{x}(t), \xi(t), t),$$

$$\frac{d\xi}{dt} = B(\mathbf{x}(t), \xi(t), t),$$

where

$$A(\mathbf{x}, \xi, t) = \mathbf{u}(\mathbf{x}, t) = \mathbf{u}_{\text{potential}}(\mathbf{x}(t), t) + (K * \xi)(\mathbf{x}(t), t)$$

and

$$B(\mathbf{x}, \xi, t) = (\xi\cdot\nabla)(\mathbf{u}_{\text{potential}}(\mathbf{x}(t), t)) + (K * \xi)(\mathbf{x}(t), t) + R^{-1}\nabla^2\xi(\mathbf{x}(t), t).$$

The second-order timestepping scheme that we used can be written as follows: We define intermediate values $\mathbf{x}^{n+1/2}$, $\xi^{n+1/2}$, which approximate $\mathbf{x}$ and ξ at time $t_{n+1/2} = (n + 1/2)\Delta t$,

$$\mathbf{x}^{n+1/2} = \mathbf{x}^n + \frac{\Delta t}{2}A(\mathbf{x}^n, \xi^n, t_n),$$

$$\xi^{n+1/2} = \xi^n + \frac{\Delta t}{2}B(\mathbf{x}^n, \xi^n, t_n).$$

The approximated values at time $t + \Delta t = (n + 1)\,\Delta t$ are then

$$\mathbf{x}^{n+1} = \mathbf{x}^n + \Delta t\, A(\mathbf{x}^{n+1/2}, \xi^{n+1/2}, t_{n+1/2}),$$

$$\xi^{n+1} = \xi^n + \Delta t\, B(\mathbf{x}^{n+1/2}, \xi^{n+1/2}, t_{n+1/2}).$$

Combining time with spatial discretization we find, for the intermediate time step $n + \frac{1}{2}$,

$$\begin{aligned}
\tilde{\mathbf{x}}_i^{n+1/2} &= \tilde{\mathbf{x}}_i^n + \frac{\Delta t}{2}\Bigg[\mathbf{u}_{\text{potential}}(\tilde{\mathbf{x}}_i^n) + \sum_j \mathbf{K}_\delta(\tilde{\mathbf{x}}_i^n - \tilde{\mathbf{x}}_j^n)\tilde{\tau}_j^n a_j \\
&\quad - \sum_j K_\delta(\tilde{\mathbf{x}}_i^n - \tilde{\mathbf{y}}_j^n)\frac{\tilde{\tau}_j^n}{|\tilde{\mathbf{x}}_j^n|}a_j\Bigg], \\
\tilde{\tau}_i^{n+1/2} &= \tilde{\tau}_i^n + \frac{\Delta t}{2}\Bigg\{(\tilde{\tau}_i^n\cdot\nabla)\mathbf{u}_{\text{potential}}(\tilde{\mathbf{x}}_i^n) \\
&\quad + \tilde{\tau}_i^n\cdot\Bigg[\sum_j \nabla K_\delta(\tilde{\mathbf{x}}_i^n - \tilde{\mathbf{x}}_j^n)\tilde{\tau}_j^n a_j \\
&\quad - \sum_j \nabla K_\delta(\tilde{\mathbf{x}}_i^n - \tilde{\mathbf{y}}_j^n)\frac{\tilde{\tau}_j^n}{|\tilde{\mathbf{x}}_j^n|}a_j\Bigg] \\
&\quad + R^{-1}\sum_j \nabla^2\phi_\delta(\tilde{\mathbf{x}}_i^n - \tilde{\mathbf{x}}_j^n)\tilde{\tau}_j^n a_j \\
&\quad - R^{-1}\sum_j \nabla^2\phi_\delta(\tilde{\mathbf{x}}_i^n - \tilde{\mathbf{y}}_j^n)\frac{\tilde{\tau}_j^n}{|\tilde{\mathbf{x}}_j^n|}a_j\Bigg\}.
\end{aligned} \tag{5.8}$$

And for the next time step, t_{n+1}, we have

$$\begin{aligned}
\tilde{\mathbf{x}}_i^{n+1} &= \tilde{\mathbf{x}}_i^n + \Delta t\Bigg[\mathbf{u}_{\text{potential}}(\tilde{\mathbf{x}}_i^{n+1/2}) + \sum_j K_\delta(\tilde{\mathbf{x}}_i^{n+1/2} - \tilde{\mathbf{x}}_j^{n+1/2})\tilde{\tau}_j^{n+1/2}a_j \\
&\quad - \sum_j K_\delta(\tilde{\mathbf{x}}_i^{n+1/2} - \tilde{\mathbf{y}}_j^{n+1/2})\frac{\tilde{\tau}_j^{n+1/2}}{|\tilde{\mathbf{x}}_j^{n+1/2}|}a_j\Bigg], \\
\tilde{\tau}_i^{n+1} &= \tilde{\tau}_i^n + \Delta t\Bigg\{(\tilde{\tau}_i^{n+1/2}\cdot\nabla)\mathbf{u}_{\text{potential}}(\tilde{\mathbf{x}}_i^{n+1/2}) \\
&\quad + \tilde{\tau}_i^{n+1/2}\cdot\Bigg[\sum_j \nabla K_\delta(\tilde{\mathbf{x}}_i^{n+1/2} - \tilde{\mathbf{x}}_j^{n+1/2})\tilde{\tau}_j^{n+1/2}a_j \\
&\quad - \sum_j \nabla K_\delta(\tilde{\mathbf{x}}_i^{n+1/2} - \tilde{\mathbf{y}}_j^{n+1/2})\frac{\tilde{\tau}_j^{n+1/2}}{|\tilde{\mathbf{x}}_j^{n+1/2}|}a_j\Bigg] \\
&\quad + R^{-1}\sum_j \nabla^2\phi_\delta(\tilde{\mathbf{x}}_i^{n+1/2} - \tilde{\mathbf{x}}_j^{n+1/2})\tilde{\tau}_j^{n+1/2}a_j \\
&\quad + R^{-1}\sum_j \nabla^2\phi_\delta(\tilde{\mathbf{x}}_i^{n+1/2} - \tilde{\mathbf{y}}_j^{n+1/2})\frac{\tilde{\tau}_j^{n+1/2}}{|\tilde{\mathbf{x}}_j^{n+1/2}|}a_j\Bigg\}.
\end{aligned} \tag{5.9}$$

There is a large variety of cutoff functions $\phi(\mathbf{x})$ that can be chosen. Since we must differentiate the cutoff function twice (see (5.8)–(5.9)), we have chosen a smooth (actually infinitely smooth) cutoff function. We have picked a fourth-order cutoff function ($d = 4$), which was suggested by Beale and Majda [12], i.e.,

$$\phi(\mathbf{x}) = \frac{3}{4\pi}\left(2e^{-r^3} - \frac{1}{2}e^{-r^3/2}\right),$$

where $r = |\mathbf{x}|$. This ensures a regularization error (the error between the exact vorticity and its convolution with the cutoff function above) of order δ^4, and error of the same order for

the three-dimensional Euler's equations. Since ϕ is a radially symmetric function, the smoothed kernel K_δ can be written in terms of K as

$$K_\delta(\mathbf{x}) = (1 - 2e^{-r^3/\delta^3} + e^{-r^3/2\delta^3})K(\mathbf{x}).$$

The cutoff function may be differentiated twice to obtain $\nabla^2\phi_\delta$,

$$\nabla^2\phi_\delta(\mathbf{x}) = \frac{3r}{4\pi\delta^6}\left[\left(18\left(\frac{r}{\delta}\right)^3 - 24\right)e^{-r^3/\delta^3} + \left(3 - \frac{9}{8}\left(\frac{r}{\delta}\right)^3\right)e^{-r^3/2\delta^3}\right],$$

and it can be readily verified that $\hat{\phi}(\mathbf{s}) \geq 0$ (see [28]). The stretching term takes the form

$$\frac{d\tilde{\tau}_i}{dt} = \sum_j [\tilde{\tau}_i^x A_\delta(\tilde{\mathbf{x}}_i - \tilde{\mathbf{x}}_j)\tilde{\tau}_j(t) + \tilde{\tau}_i^y B_\delta(\tilde{\mathbf{x}}_i - \tilde{\mathbf{x}}_j)\tilde{\tau}_j(t) + \tilde{\tau}_i^z C_\delta(\tilde{\mathbf{x}}_i - \tilde{\mathbf{x}}_j)\tilde{\tau}_j(t)]a_j,$$

where

$$a_j = a^2\,\Delta\theta\,\Delta\phi\,(\sin\theta_j)_{\text{original}},$$

$\tilde{\tau}_i = (\tilde{\tau}_i^x, \tilde{\tau}_i^y, \tilde{\tau}_i^z)$, and

$$A_\delta(\mathbf{x}) = \frac{\partial}{\partial x}K_\delta(\mathbf{x}), \quad B_\delta(\mathbf{x}) = \frac{\partial}{\partial y}K_\delta(\mathbf{x}), \quad C_\delta(\mathbf{x}) = \frac{\partial}{\partial z}K_\delta(\mathbf{x}).$$

Or more explicitly,

$$\tilde{\tau}_i^x A_\delta(\mathbf{x})\tilde{\tau}_j = \tilde{\tau}_i^x\left(F_{1\delta}\left(\frac{-(r^2-3x^2)}{4\pi r^5}\right), F_{2\delta}\left(\frac{3xy}{4\pi r^5}\right), F_{3\delta}\left(\frac{3xz}{4\pi r^5}\right)\right) \times \tilde{\tau}_j$$

$$\tilde{\tau}_i^y B_\delta(\mathbf{x})\tilde{\tau}_j = \tilde{\tau}_i^y(G_{1\delta}\left(\frac{3yx}{4\pi r^5}\right), G_{2\delta}\left(\frac{-(r^2-3y^2)}{4\pi r^5}\right), G_{3\delta}\left(\frac{3yz}{4\pi r^5}\right)\right) \times \tilde{\tau}_j$$

$$\tilde{\tau}_i^z C_\delta(\mathbf{x})\tilde{\tau}_j = \tilde{\tau}_i^z\left(H_{1\delta}\left(\frac{3zx}{4\pi r^5}\right), H_{2\delta}\left(\frac{3zy}{4\pi r^5}\right), H_{3\delta}\left(\frac{-(r^2-3z^2)}{4\pi r^5}\right)\right) \times \tilde{\tau}_j.$$

Here $F_{i\delta}, G_{i\delta}, H_{i\delta}$ for $i = 1, 2, 3$ indicate smoothing operators on the corresponding functions. For example,

$$F_{1\delta}\left(\frac{-(r^2-3x^2)}{4\pi r^5}\right) = -\frac{1}{4\pi r^5}\left[(r^2-3x^2) - 2e^{-r^3/\delta^3}\left(r^2 - 3x^2\left(1+\frac{r^3}{\delta^3}\right)\right) + e^{-r^3/2\delta^3}\left(r^2 - 3x^2\left(1+\frac{1}{2}\frac{r^3}{\delta^3}\right)\right)\right]$$

and

$$F_{2\delta}\left(\frac{3xy}{4\pi r^5}\right) = \frac{3xy}{4\pi r^5}\left[\left(1 - 2e^{-r^3/\delta^3}\left(1+\frac{r^3}{\delta^3}\right) + e^{-r^3/2\delta^3}\left(1+\frac{1}{2}\frac{r^3}{\delta^3}\right)\right)\right].$$

Other smoothing functions can be similarly derived; i.e., smoothing of terms which include $r^2 - 3y^2$ and $r^2 - 3z^2$ are similar to the one for $r^2 - 3x^2$, and smoothing for terms which include $3xz$ and $3yz$ are similar to the one for $3xy$.

6. BOUNDARY CONDITIONS

The boundary conditions that should be supplied to the differential equations arise from the boundaries of the physical domain $r \geq a$ and from the artificial boundary at $r = b$. In fact, we are solving two systems of differential equations; one in the domain $r \geq b$, and the second in $a \leq r \leq b$. For the first region $r \geq b$ we impose

(a) the far field boundary condition $\mathbf{u} \to \mathbf{U}$ at $r \to \infty$; this is satisfied by the addition of a potential flow field (see (5.4));

(b) the continuity conditions for u_θ, u_ϕ and ξ_θ, ξ_ϕ at $r = b$; these conditions will be expanded upon later in this section.

In the second region $a \leq r \leq b$ we apply

(a) the no-slip boundary condition $u_\theta = u_\phi = 0$ on $r = a$ by vorticity creation (see (4.10a)–(4.10b));

(b) the no-leak boundary condition $u_r = 0$ by creating imaginary blobs (see (5.7)) and by constructing u_r from u_θ and u_ϕ via the incompressibility condition (see (4.7));

(c) boundary conditions on u_θ and u_ϕ at $r = b$ by prescribing their values subjected to the interior flow (see (4.8)–(4.9) and [27]); and

(d) smooth transition of the tangential components of the vorticity vector on $r = b$; this process is described below.

The transition between the two regions is done as follows: A tile that crosses $r = b$ becomes a blob, which shares the same vorticity with the corresponding tile; i.e., ξ_θ, ξ_ϕ, and $\xi_r = 0$ are transformed continuously, while its Cartesian repre-

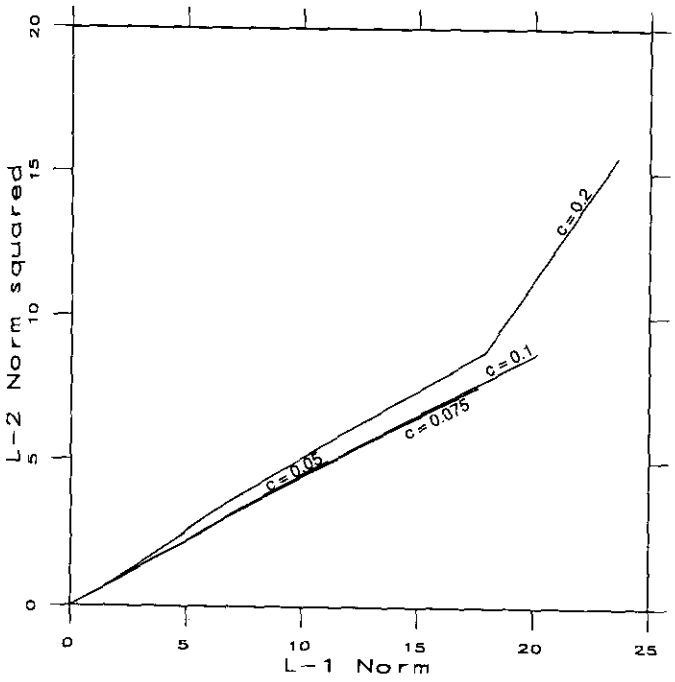

FIG. 1. Discretized $\|\xi\|_2^2$ versus discretized $\|\xi\|_1$.

sentation of ξ is given by (4.11a)–(4.11c). Similarly, if a blob passes the border $r = b$, it becomes a tile, which has zero radial component, and its tangential components are expressed via the inverse of the transformation (4.11a)–(4.11c).

7. ON THE CONVERGENCE OF THE SCHEME

Several theorems have been proved on the convergence of vortex schemes to two- or three-dimensional Euler's equations (see, for example, [32, 10, 11, 46, 22, 8]). Beale [8] has bounded the errors in a three-dimensional vortex scheme with grid-free stretching (the same scheme presented here but without viscous terms). Assuming that the velocity field is smooth for $0 \le t \le T$ and the initial vorticity field ξ_0 is compactly supported, he showed that if one picks a cutoff function of order $d \ge 4$ and a cutoff parameter $\delta = c_0 h^q$ for fixed c_0 and $\frac{1}{3} < q < 1$, then for $0 \le t \le T$, $1 < p < \infty$,

TABLE I

Time	$\|\xi\|_1$	$\|\xi\|_2^2$	max|u|	max|r|	No. (tiles, blobs)
0.38	$1.90 * 10^2$	$8.65 * 10^1$	3.623	0.7851	(904,0)
0.62	$3.32 * 10^2$	$1.52 * 10^2$	5.071	0.7865	(1543,52)
0.89	$6.87 * 10^2$	$3.53 * 10^2$	10.231	12.349	(2857,472)
1.04	$1.36 * 10^3$	$7.18 * 10^2$	11.406	20.512	(5605,832)
1.15	$2.24 * 10^3$	$1.18 * 10^3$	13.988	26.916	(9297,1178)
1.21	$2.62 * 10^3$	$1.41 * 10^3$	14.853	30.372	(10745,1552)

TABLE II

Time	$\|\xi\|_1$	$\|\xi\|_2^2$	E_i	No. (tiles, blobs)
0.78	$1.98 * 10^2$	$4.57 * 10^2$	$1.46464 * 10^3$	(1671,281)
1.57	$7.38 * 10^2$	$6.51 * 10^2$	$1.46968 * 10^3$	(2300,1976)
1.82	$1.43 * 10^3$	$1.09 * 10^3$	$1.46482 * 10^3$	(6269,3691)
2.22	$2.86 * 10^3$	$2.64 * 10^3$	$1.47033 * 10^3$	(8874,10376)
2.41	$3.99 * 10^3$	$3.82 * 10^3$	$1.46962 * 10^3$	(12045,14858)

$$\|\tilde{\mathbf{x}}_i(t) - \mathbf{x}_i(t)\|_{0,p,h} \le C\delta^d, \quad \|\tilde{\xi}_i(t) - \xi_i(t)\|_{-1,p,h} \le C\delta^d.$$

Here the norms $\|\cdot\|_{0,p,h}$, $\|\cdot\|_{-1,p,h}$ are the discrete $L^p(R^3)$ and $W^{-1,p}(R^3)$ norms, respectively.

Concerning viscous effects, convergence of a deterministic vortex scheme to the convection-diffusion equation $\partial\xi/\partial t + (\mathbf{a}(\mathbf{x}, t) \cdot \nabla)\xi = R^{-1}\Delta^2\xi$ has been established [24, 29]. We have the following.

THEOREM [29]. *Let $\phi \in W^{m+5,1}(R^2)$, $m \ge d + 2$, be a cutoff function of order d with non-negative Fourier transform, i.e., $\hat{\phi}(\mathbf{s}) = \int_{R^2} \phi(\mathbf{x})e^{-i\mathbf{x}\cdot\mathbf{s}}\, d\mathbf{x} \ge 0$. Assume that $\mathbf{a}(\mathbf{x}, t)$ and the transformation from α to $\mathbf{x}$ via the flow map has continuous and uniformly bounded derivatives to order $m + 3$ and that $\xi \in W^{m+3,2}(R^2)$, $m \ge d + 2$. Define the approximate solution $\tilde{\xi}_i(t)$ as*

$$\frac{d\mathbf{x}_i(t)}{dt} = \mathbf{a}(\mathbf{x}_i, t), \quad \text{div } \mathbf{a} = 0,$$

$$\frac{d\tilde{\xi}_i(t)}{dt} = R^{-1} \sum_j \Delta\phi_\delta(\mathbf{x}_i(t) - \mathbf{x}_j(t))\tilde{\xi}_j(t)h^2,$$

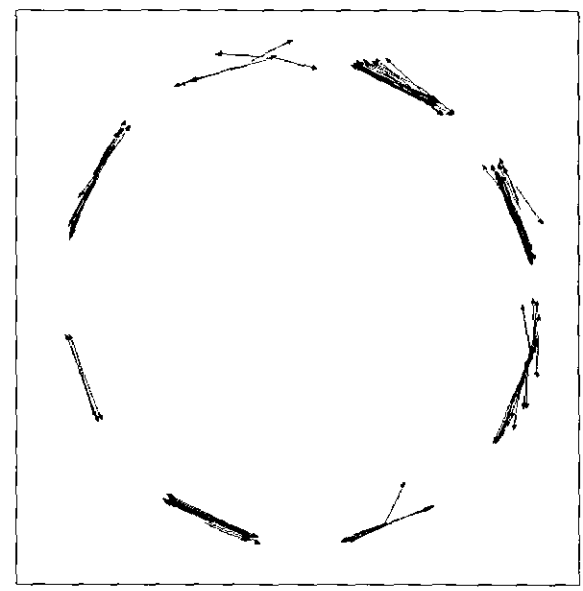

FIG. 2. Vorticity field projected on (x, z) plane $y = 0$ at $t = 0.38$.

FIG. 3. Vorticity field projected on (x, z) plane $y = 0$ at $t = 1.04$.

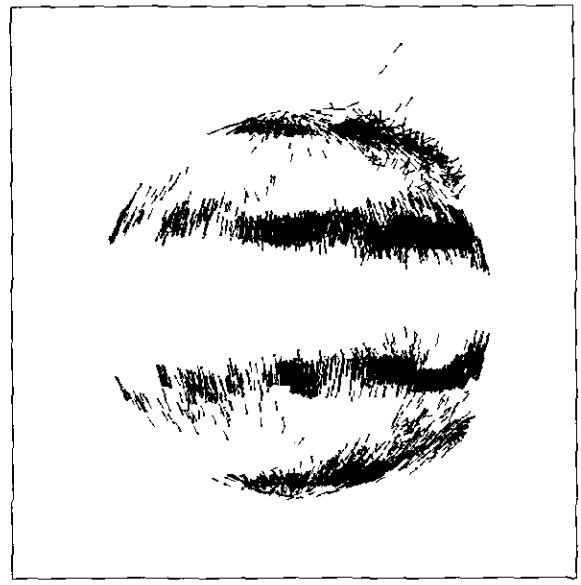

FIG. 5. Vorticity field at $t = 1.04$.

where $\mathbf{x}_i(0)$ *are uniformly distributed points in* R^2 *with mesh-spacing* h, *and* $\tilde{\xi}_i(0) = \xi(\mathbf{x}_i(0), 0)$. *Then*

$$\|\tilde{\xi} - \xi\|_{0,2,h} \leq C(t)R^{-1}\left(\delta^d + \frac{h^m}{\delta^{m+2}}\right),$$

where $C(t)$ *depends on* t *and on the* $W^{k,2}$*-Sobolev norms* $\|\xi\|_{k,2}$, $0 \leq k \leq m + 3$, *at the initial time* $t = 0$. *Convergence can be extended to the three-dimensional problem* $\partial\xi/\partial t + (\mathbf{a}(\mathbf{x}, t)\cdot\nabla)\xi = (\xi\cdot\nabla)\mathbf{a}(\mathbf{x}, t) + R^{-1}\nabla^2\xi$, *with similar bounds on the error assuming that* $\mathbf{a}$ *and* $\nabla\mathbf{a}$ *are smooth enough.*

Goodman [30] and Long [35] have proved the convergence of a random-vortex scheme to the two-dimensional Navier–Stokes equations. A convergence proof for the scheme in the boundary layer is not available yet; however, a numerical study of the vortex sheet method for the Prandtl equations [45] indicates that the error between the approximated steady solution and the Blasius solution is of order $(h + \xi_{\max})\sqrt{\Delta t/R}$, where h is the initial spacing in the streamwise direction and ξ_{max} is the

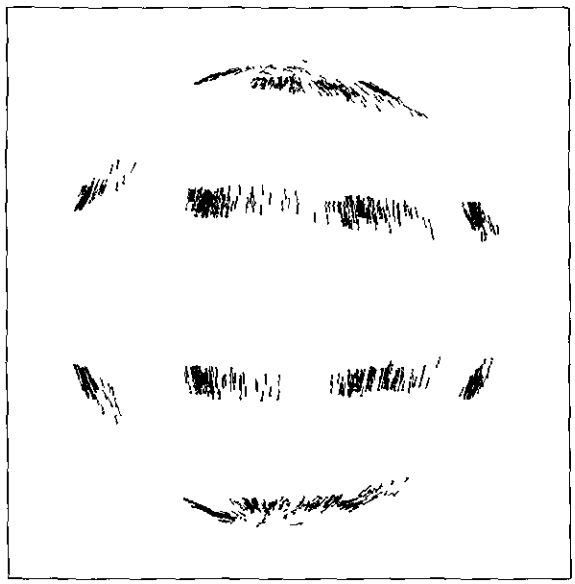

FIG. 4. Vorticity field at $t = 0.38$.

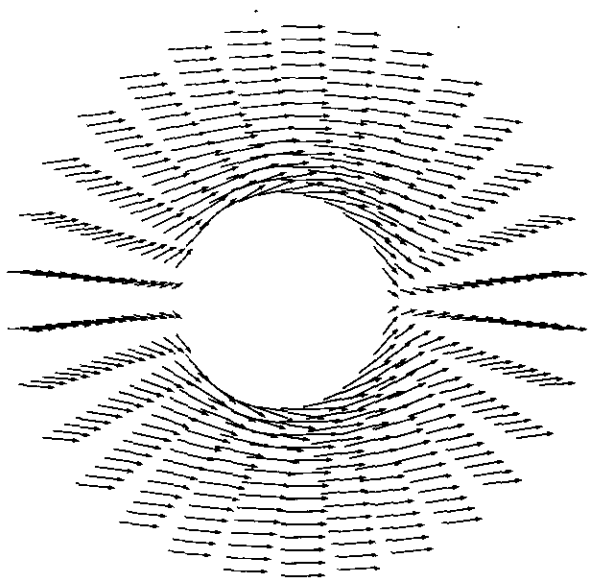

FIG. 6. Velocity field projected on (x, z) plane $y = 0$ at $t = 0.38$.

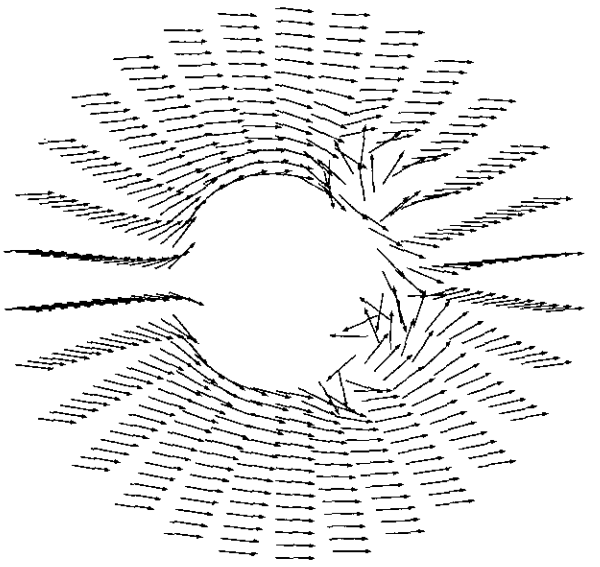

FIG. 7. Velocity field projected on (x, z) plane $y = 0$ at $t = 1.04$.

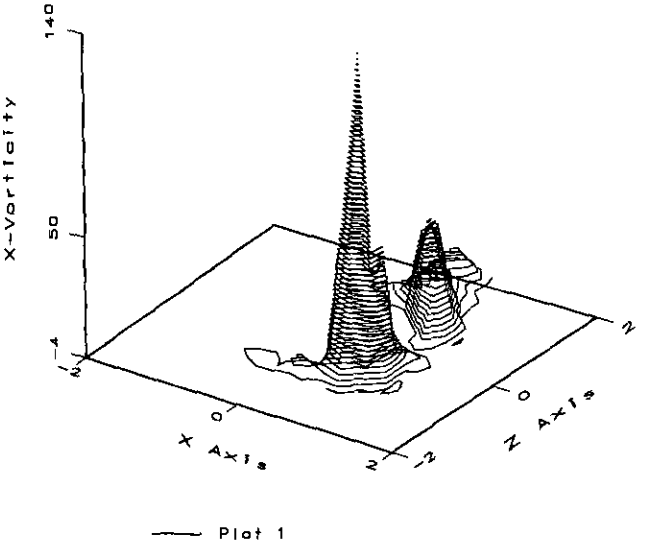

FIG. 9. Streamwise vorticity contours projected on (x, z) plane at $t = 1.04$.

maximal vorticity of newly created sheets. A one-dimensional analysis for the heat equations with vorticity-creation [31] provides the estimate $P(\|\tilde{u} - u\|_{L^2}/\|u\|_{L^2} \leq C_R(\Delta t/t + k/\sqrt{N})) \geq 1 - 1/k^2$, where N in the number of tiles, k is an arbitrary positive number, and P denotes probability.

8. RESULTS

We present results for a flow over a sphere of radius 1 ($a = 1$) and Reynolds number 3000. This number was found to be high enough to exhibit turbulence phenomena, such as growth in the vorticity L_1 and L_2 norms and the creation of very small scales of vorticity as well as velocity. Similar results, although more profound, can be found for higher Reynolds numbers. We have tried several spatial and temporal meshes, and the one for which we represent the results was fine enough to capture the vorticity growth in the discretized L_1 and L_2 norms and coarse enough to make our computations affordable for at least a time interval of order one. In Fig. 1 computed values for $(\|\xi\|_{L_1}, \|\xi\|^2_{L_2})$ for the same spatial mesh $\Delta\theta = \Delta\phi = \pi/4$ and different temporal meshes: $\max|\mathbf{u}|\ \Delta t \leq C\ \Delta\theta$ with $C = 0.2, 0.1, 0.075, 0.05$, respectively, are displayed. It is

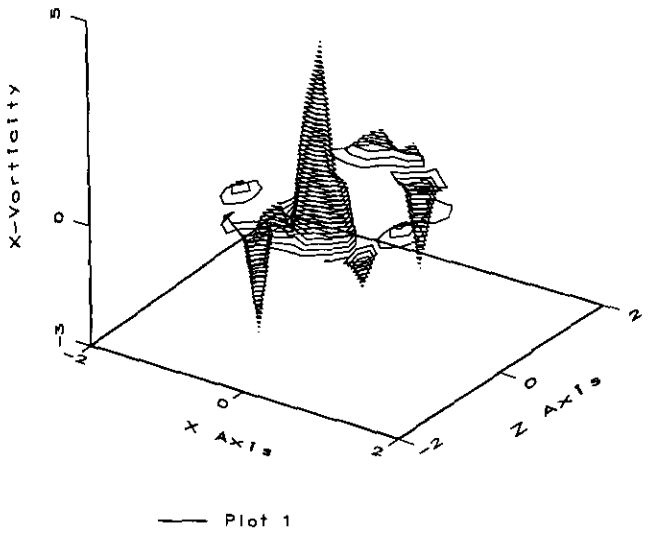

FIG. 8. Streamwise vorticity contours projected on (x, z) plane at $t = 0.38$.

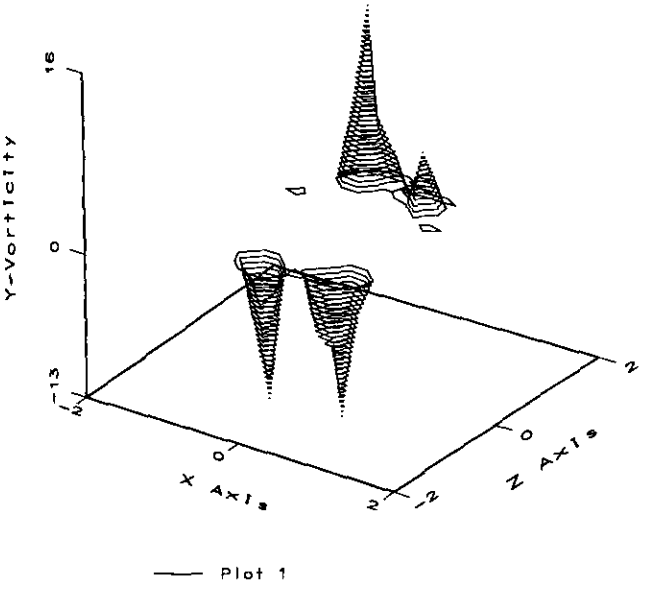

FIG. 10. Spanwise vorticity contours projected on (x, z) plane at $t = 0.38$.

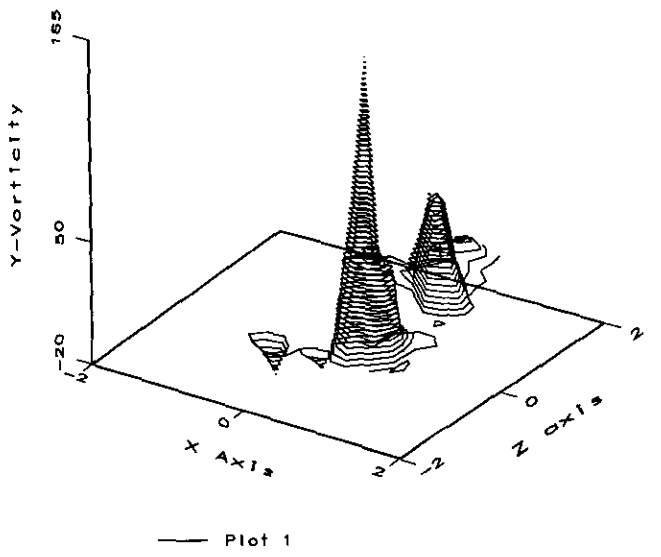

FIG. 11. Spanwise vorticity contours projected on (x, z) plane at $t = 1.04$.

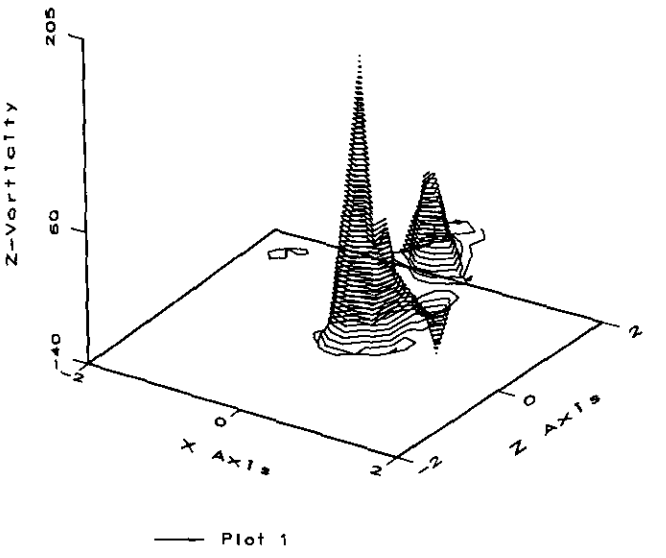

FIG. 13. Z-vorticity contours projected on (x, z) plane at $t = 1.04$.

observed that for the first 60 iterations the graph for $C = 0.1$ does not differ a lot from the ones for $C = 0.075$ and $C = 0.05$, but it does differ from the one for $C = 0.2$; therefore we picked $C = 0.1$.

Choosing the spacing in θ and ϕ to be $\Delta\theta = \pi/4$ and $\Delta\phi = 2\pi/8$, respectively, means that the no-slip boundary condition is approximately satisfied on the mesh points above, by the creation of tiles whose maximum intensity does not exceed a prescribed value $\tau_{\max}$. We have picked $\tau_{\max}$, the maximum strength of vorticity created on the boundary to be $\tau_{\max} = 0.5 * \Delta\theta$ (see [16, 27]). With these parameters we could carry out our computations for a reasonable period of time

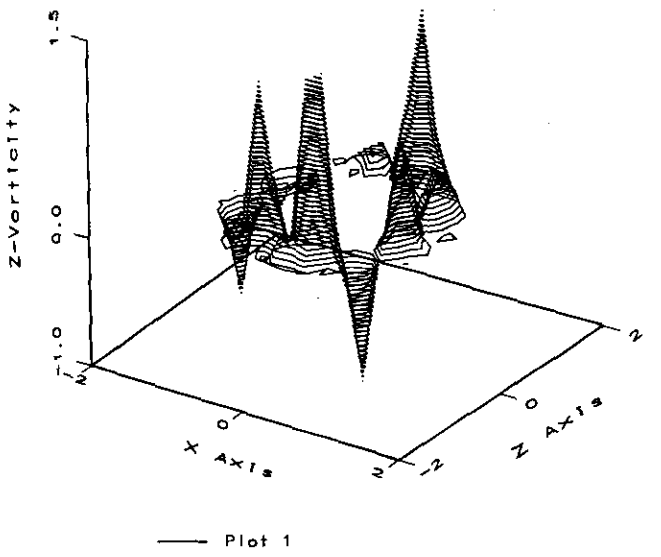

FIG. 12. Z-vorticity contours projected on (x, z) plane at $t = 0.38$.

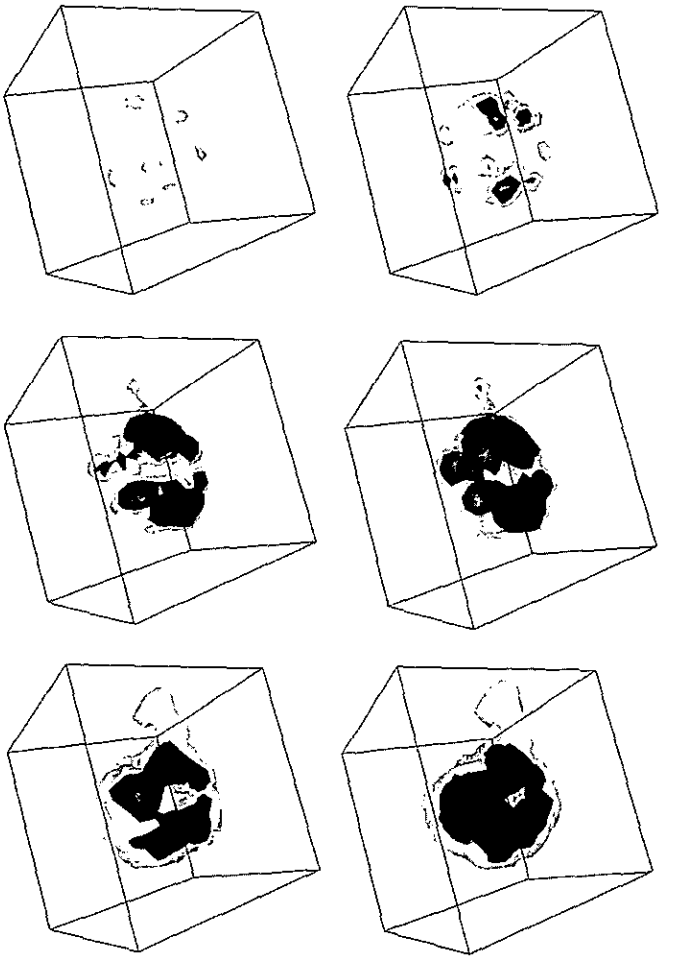

FIG. 14. Isosurfaces of vorticity-strength at levels 12.5 (light gray) and 27 (125 for the two highest time-levels) (black) at $t = 0.60, 0.77, 1.04, 1.20, 1.82, 2.41$, going from left to right, top to bottom.

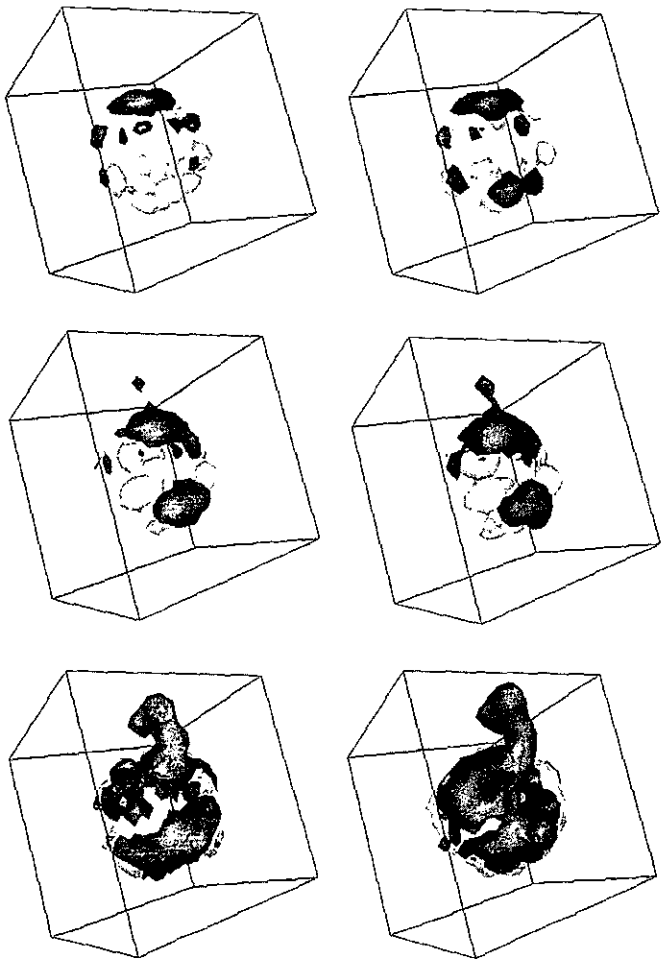

FIG. 15. Isosurfaces of spanwise vorticity at levels 4 (dark gray) and −4 (light gray) at $t = 0.60, 0.77, 1.04, 1.20, 1.82, 2.41$.

(up to $t = 1.2$), without exhausting the computing resources. Further refinement of the spatial mesh will cause a considerable growth in computing power that is needed for advancing the solution to $t = O(1)$. The scheme is numerically stable for this period of time and interesting physical phenomena have been observed. The enstrophy—the integral of $\xi \cdot \xi$ over the whole space—is, generally speaking, growing constantly as time progresses; this phenomenon was also observed in [17]. In Table I we show the growth of the discretized L_1 and L_2 norms of the vorticity as time evolves. We also show the evolution of $\max|\mathbf{u}|$ and $\max|\tau|$ and indicate the numbers of tiles and blobs as a function of time. Thus constant growth in the infinity norms of $\mathbf{u}$ and ξ is observed, and this may lead to a non-smooth velocity field as R tends to infinity in case the vorticity-strength blows up (see [9]).

In Table II we show flow quantities for a longer-time simulation, this time with $\tau_{\max} = 0.025 * \Delta\theta$ and $\Delta t = C(t) * \Delta\theta$, where $C(t)$ is decreasing from 0.1 to 0.025 as the time evolves. Further progress in time can be made as soon as a fast summation method is applied to reduce the cost of the velocity field computation. In Table II we show the evolution of the kinetic energy E_k defined on a bounded domain $B_0 = \{\mathbf{x} | a \le |\mathbf{x}| \le R_0\}$ as a function of time; one can observe that it fluctuates about the same value. Looking at the rate of change of the kinetic energy defined on the bounded domain B_0, with boundary ∂B_0, we find that

$$\frac{\partial}{\partial t}\frac{1}{2}\int_{B_0} \mathbf{u}\cdot\mathbf{u}\, d\mathbf{x} = -\frac{1}{2}\int_{\partial B_0} (\mathbf{u}\cdot\mathbf{u})(\mathbf{u}\cdot\mathbf{n})\, dS + \int_{\partial B_0} p(\mathbf{u}\cdot\mathbf{n})\, dS + \int_{\partial B_0} (\nabla\mathbf{u}\,\mathbf{u})\cdot\mathbf{n}\, dS - R^{-1}\int_{B_0} |\nabla\mathbf{u}|^2\, d\mathbf{x},$$

where $|\nabla\mathbf{u}|^2 = |\nabla u|^2 + |\nabla v|^2 + |\nabla w|^2$. The contributions of the boundary integral from the sphere $r = a$ are zero since all components of the velocity field vanish there. If R_0 is large, then $\mathbf{u}$ is nearly the potential velocity on $r = R_0$; thus $\mathbf{u}\cdot\mathbf{n}$ is nearly $U(x/r)(1 - a^3/r^3)$, which is antisymmetric with respect to x. Thus the first integral on $r = R_0$ vanishes for the potential flow field, and

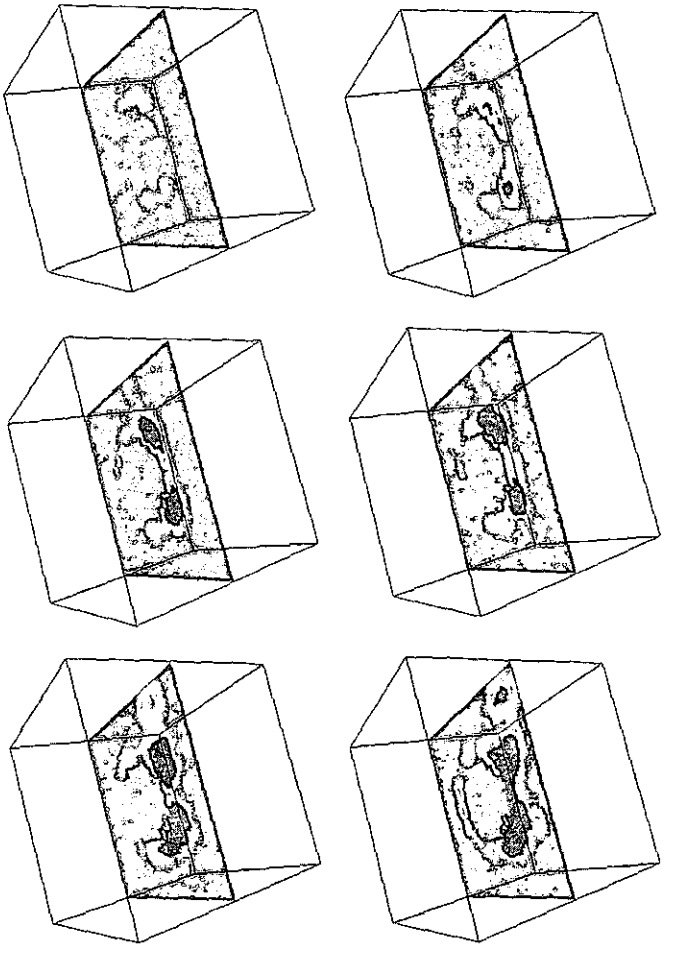

FIG. 16. Contours of vorticity-strength on the plane $y = 0.09$ (dark gray represents intense vorticity) at $t = 0.60, 0.77, 1.04, 1.20, 1.82, 2.41$.

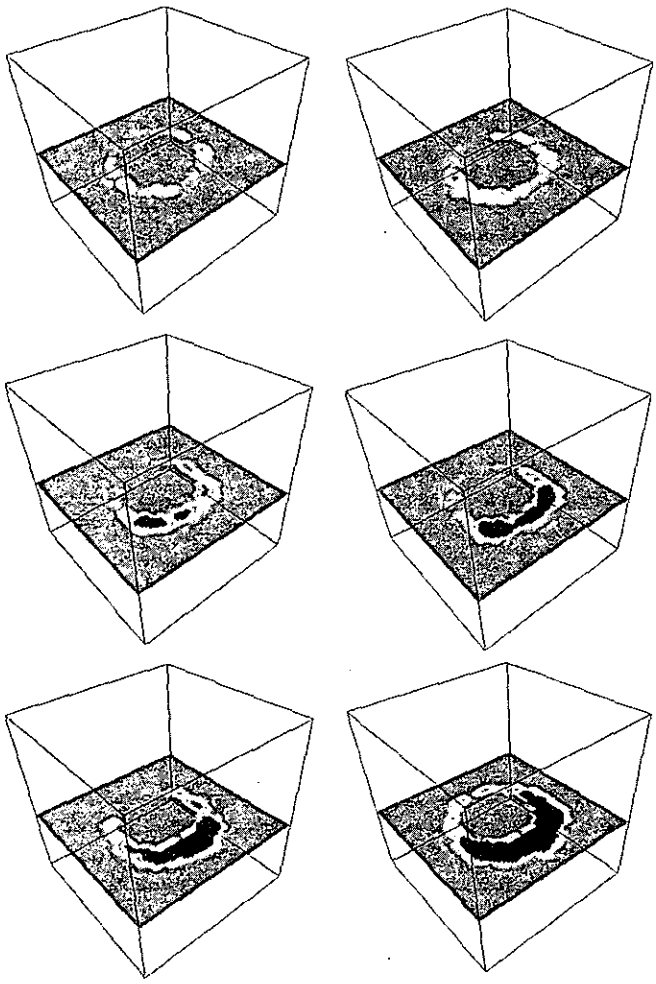

FIG. 17. Contours of vorticity-strength on the plane $z = -0.2$ (dark gray represents intense vorticity) at $t = 0.60, 0.77, 1.04, 1.20, 1.82, 2.41$.

the same is true for the second integral, since p is symmetric with respect to x. As for the third integral, it is easy to see that it decays as $O(R_0^{-2})$ for the potential flow-field. In the numerical simulation one can observe small fluctuations of the kinetic energy about its mean value; this is probably caused by numerical errors and due to the contributions of our finite domain.

In Figs. 2 and 3 we represent the vorticity field projected on the x, z plane at early ($t = 0.388$) and more developed stages ($t = 1.04$) of the flow, respectively. We observe that while in the beginning the vorticity vector was tangential to the sphere, it is later oriented in various directions and it grows in magnitude in several regions of the flow. Figures 4 and 5 display the vorticity field in the whole space at $t = 0.388$ and $t = 1.04$, respectively. In Figs. 6 and 7 we display the projection of the velocity field at the same time stages as in Figs. 2 and 3, respectively. For the more developed stage, uniform magnitudes but varying directions of the velocity field are represented. Since the vorticity field is represented by a linear combination of velocity gradients, it is plausible to expect that in certain regions the magnitude of the velocity gradients grows in time; this phenomena is observed in Fig. 5. Moreover, the velocity field deviates a lot from the potential field that corresponds to the flow over the sphere. In Figs. 8 and 9 we show streamwise vorticity contours in the x, z plane for $t = 0.388$ and $t = 1.04$, respectively. Similarly, Figs. 10 and 11 represent spanwise vorticity contours, and Figs. 12 and 13 represent contours of the z-component of the vorticity vector. One notes that as time evolves the vorticity is concentrated in more restricted portions of the physical domain and this suggests that the Hausdorff dimension of the support of the vorticity is less than three.

Figures 14–17 represent vorticity isosurfaces and contours at $t = 0.60, 0.77, 1.04, 1.20, 1.82$, and 2.41; for the last two time levels the parameters were chosen as for Table II. Figure 14 displays isosurfaces of vorticity strength at levels 12.5 (light gray) and 27 (black) for different time levels, where for the last two time levels the isosurface levels are 12.5 and 125 (instead of 27). The flow is coming from the left towards the viewer on the right. One can note how the vorticity-strength is spreading out over the sphere and then away from it as time

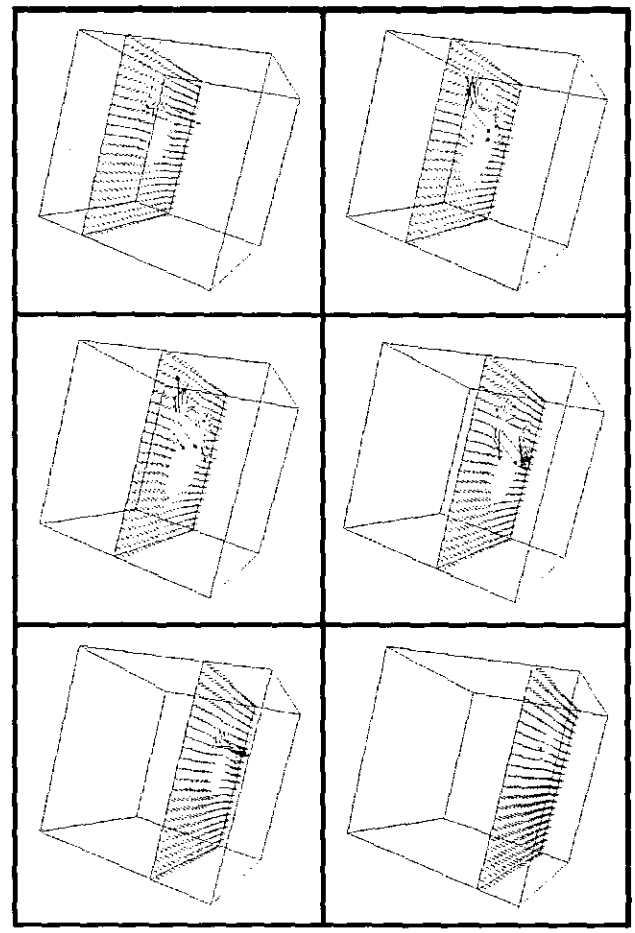

FIG. 18. Velocity field on the planes $x = -0.4, 0., 0.4, 0.8, 1.2$ at $t = 1.04$; the order is from left to right and top to bottom.

develops. In Fig. 15 spanwise-vorticity isosurfaces at levels 4 (dark gray) and -4 (light gray) are displayed; note that some antisymmetry is retained in the initial stages, but is broken later in time, since the numerical processes (especially the stochastic ones) introduce antisymmetric disturbances that grow in the course of the time evolution.

In Fig. 16 I have plotted vorticity-strength contours on the plane $y = 0.09$; dark areas represent intense vorticity. It is seen that two main vortices, which cause circulation of the fluid, are formed in the rear of the sphere. This figure shows a similarity to known numerical and physical results for the flow over a cylinder at high Reynolds numbers (see, for example, [15]) and it makes us more confident that the numerical results are giving a physically realistic simulation. Similarly, Fig. 17 displays vorticity-strength contours at $z = -0.2$ at different time levels. Note the formation of a variety of vortices near the surface of the sphere and the way they become more intense in the rear of the sphere as time progresses.

Figures 18–20 display the velocity field on selected planes for $t = 1.04$. Figure 18 contains the planes $x = -0.8, -0.4,$ 0., 0.4, 0.8, and 1.2. Note that away from the sphere, at $x = 1.2$, for example, the flow becomes more regular and is dominated by the far-field conditions. At $x = -0.4$, 0., 0.4 there are disturbances which are due to vorticity-creation on the sphere. Similar such graphics were presented in the paper of Bernard *et al.* [13] for vertex identification. For Fig. 19 the selected planes are $y = -0.8, -0.4$, 0., 0.4, 0.8, and 1.2; circulation of the fluid on y-planes represents spanwise-vorticity formation. Figure 20 displays the velocity-field on the z-planes $z = -0.4$, 0., 0.4, 0.8, 1.2; irregular flow, which is caused by vorticity concentration, is taking place for some of these planes.

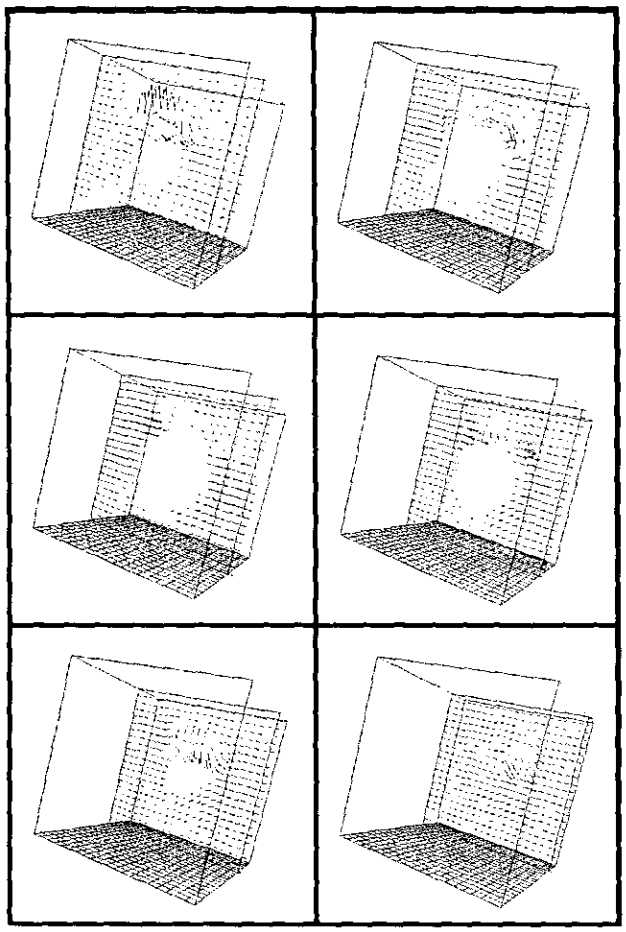

FIG. 19. Velocity field on the planes $y = -0.4$, 0., 0.4, 0.8, 1.2 at $t = 1.04$; the order is from left to right and top to bottom.

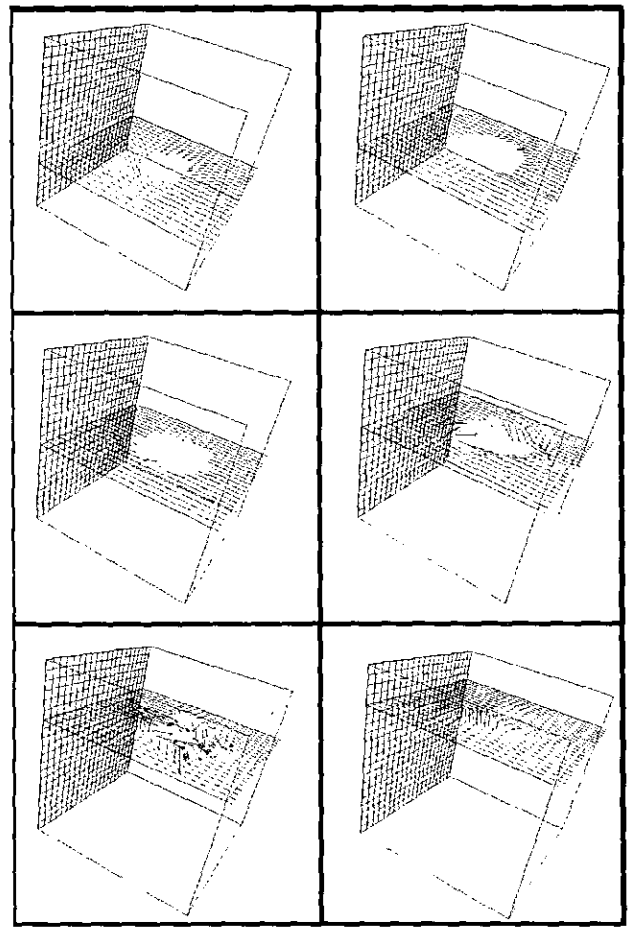

FIG. 20. Velocity field on the planes $z = -0.4$, 0., 0.4, 0.8, 1.2 at $t = 1.04$; the order is from left to right and top to bottom.

ACKNOWLEDGMENTS

Research was supported in part by the Robert Szold Institute for Applied Science of the P.E.F. Israel Endowment Funds, and in part by the Landau Center for Mathematical Research in Analysis supported by Minerva Foundation (Germany). It is a pleasure to thank the Center for Visualization of Dynamic Systems, The Hebrew University, for providing advanced (AVS) graphics tools. I thank the referees and M. Ben-Artzi for helpful comments on the paper.

REFERENCES

1. C. Anderson and C. Greengard, *SIAM J. Numer. Anal.* **22,** 413 (1985).
2. W. Ashurst, A. Kerstein, R. Kerr, and C. Gibson, *Phys. Fluids* **30,** 2343 (1987).
3. M. Avellaneda and A. Majda, *Commun. Math. Phys.* **131,** 381 (1990).
4. M. Avellaneda and A. Majda, *Commun. Math. Phys.*, submitted.
5. S. B. Baden and E. G. Puckett, *J. Comput. Phys.* **37** (1990).
6. G. K. Batchelor, *An Introduction to Fluid Dynamics* (Cambridge Univ. Press, Cambridge, United Kingdom, 1970).
7. G. K. Batchelor, *The Theory of Turbulence* (Cambridge Univ. Press, Cambridge, United Kingdom, 1956).
8. T. Beale, *Math. Comput.* **46,** 401 (1986).
9. J. T. Beale, T. Kato, and A. J. Majda, *Commun. Math. Phys.* **94,** 61 (1984).
10. T. Beale and A. Majda, *Math. Comput.* **39,** 1 (1982).
11. T. Beale and A. Majda, *Math. Comput.* **39,** 29 (1982).
12. T. Beale and A. Majda, *J. Comput. Phys.* **58,** 188 (1985).
13. P. Bernard, J. Thomas, and R. Handler, *J. Fluid Mech.*, to appear.
14. R. Bouard and M. Coutanceau, *J. Fluid Mech.* **101,** 583 (1980).
15. A. Y. Cheer, *J. Fluid Mech.* **201,** 485 (1989).
16. A. J. Chorin, *SIAM J. Sci. Statist. Comput.* **1,** 1 (1980).
17. A. J. Chorin, The evolution of a turbulent vortex, *Commun. Math. Phys.* **83,** 517 (1982).
18. A. J. Chorin, in *Vortex Flows,* edited by K. Gustafson and J. Sethian (SIAM, Philadelphia, 1990).
19. A. J. Chorin, *J. Comput. Phys.* **91,** 1 (1990).
20. A. J. Chorin, *Lectures on Turbulence Theory,* Math. Lecture Series, Vol. 5 (Publish or Perish, Boston, 1975).
21. P. Constantin and A. Majda, *Commun. Math. Phys.* **115,** 435 (1988).
22. G. H. Cottet, *Ann. Inst. Henri Poincaré, Anal. Non lineaire.*
23. M. Coutanceau and R. Bouard, *J. Fluid Mech.* **79,** 257 (1977).
24. P. Degond and S. Mas-Gallic, *Math. Comput* **53**(188), 485 (1990).
25. P. G. Drazin and W. H. Reid, *Hydrodynamics Stability* (Cambridge Univ. Press, Cambridge, United Kingtom, 1981).
26. M. R. Head and P. Bandyapodhyay, *J. Fluid Mech.* **107,** 297 (1981).
27. D. Fishelov, Vortex methods for slightly viscous three-dimensional flow, *SIAM J. Sci. Statist. Comput.* **11,** 399 (1990).
28. D. Fishelov, *J. Comput. Phys.* **86,** 211 (1990).
29. D. Fishelov, Preprint No. 2, The Edmond Landau Center for Research in Mathematical Analysis, 1993 (unpublished).
30. J. Goodman, *Commun. Pure Appl. Math.* **40**(2), 189 (1977).
31. O. H. Hald, *SIAM J. Sci. Stat. Comput.* **7,** 1373 (1986).
32. O. Hald and V. Del Prete, *Math. Comput.* **32,** 791 (1978).
33. L. D. Landau and E. M. Lifshitz, *Fluid Mechanics* (Pergamon, Elmsford, New York, 1959).
34. C. C. Lin, *The Theory of Hydrodynamics Stability* (Cambridge Univ. Press, Cambridge, United Kingdom, 1966).
35. D.-G. Long, *J. Am. Math. Soc.* **1,** No. 4 (1988).
36. A. E. Love, *A Treatise on Mathematical Theory of Elasticity,* 4th ed. Cambridge Univ. Press, Cambridge, United Kingdom, 1927), p. 90.
37. A. J. Majda, Vorticity, turbulence and acoustics in fluid flow, *SIAM Rev.* **33**(3), 349 (1991).
38. A. J. Majda, *Commun. Pure Appl. Math.* **39,** S187 (1986).
39. B. Mandelbrot, in *Turbulence and Navier–Stokes Equations,* edited by R. Temam (Springer-Verlag, New York, 1976).
40. B. Mandelbrot, *Fractals: Form, Change and Dimension* (Freeman, San Francisco, 1977).
41. M. E. O'Neill and F. Chorlton, *Viscous and Compressible Fluid Dynamics* (Ellis Horwood, Chichester, 1989), p. 88.
42. S.-I. Pai, *Viscous Flow Theory. Part I. Laminar Flow* (Van Nostrand, Princeton, New Jersey, 1956), p. 40.
43. R. Pelz, V. Yakhot, S. Orszag, L. Shtilman, and E. Levich, *Phys. Rev. Lett.* **54,** 2505 (1985).
44. T.-P. Loc and R. Bouard, *J. Fluid Mech.* **160** (1985).
45. E. G. Puckett, *SIAM J. Sci. Statist. Comput.* **10,** 298 (1989).
46. P. A. Raviart, in *Numerical Methods in Fluid Dynamics,* Lecture Notes in Mathematics, Vol. 1127, edited by F. Brezzi (Springer-Verlag, Berlin, 1985).
47. Z. She, E. Jackson, and S. Orszag Vortex dynamics and isotropic turbulence, *J. Fluid Mech.*, submitted.
48. Wieselsberger, *Z. Flugtech. Motorluftschiffaht* **5,** 142 (1914).
49. V. Yakhot and S. Orszag, *J. Sci. Comput.* **1,** 3 (1986).